UNIVERSIDADE D
COIMBRA

Rafael da Costa Gaspar

TORQUE AND TEMPERATURE ANALYSIS IN FSSW OF ALUMINIUM ALLOYS

Dissertação no âmbito do Mestrado Integrado em Engenharia Mecânica, no ramo de Produção e Projeto orientada pelo Professor Doutor Carlos Miguel Almeida Leitão e pelo Professor Doutor Sree S.Sabari e apresentada ao Departamento de Engenharia Mecânica da Faculdade de Ciências e Tecnologia da Universidade de Coimbra

Outubro / 2020

1 2 9 0

FACULDADE DE CIÊNCIAS E TECNOLOGIA
UNIVERSIDADE D COIMBRA

TORQUE AND TEMPERATURE ANALYSIS IN FSSW OF ALUMINIUM ALLOYS

Submitted in Partial Fulfilment of the Requirements for the Degree of Master in Mechanical Engineering in the speciality of Production and Project

Análise do Binário e da Temperatura em *FSSW* de Ligas de Alumínio

Author

Rafael da Costa Gaspar

Advisors

Doutor Carlos Miguel Almeida Leitão

Doutor Sree S. Sabari

Jury

President	**Professora Doutora Cristina Maria Gonçalves dos Santos** **Professor Auxiliar da Universidade de Coimbra**
Vowel	**Professor Doutor Ivan Rodolfo Pereira Garcia de Galvão** **Professor Adjunto do Instituto Superior de Engenharia de Lisboa**
Advisor	**Professor Doutor Carlos Miguel Almeida Leitão** **Investigador Doutorado da Universidade de Coimbra**

Coimbra, October, 2020

“A tudo se chega, se a vida dura”
Maria dos Anjos

ACKNOWLEDGEMENTS

The realization of this work would not have been possible without the support and collaboration of some people, whom I could not forget to thank:

First of all, to my family, in special to my parents, Daniel and Isabel, for taking me here. I wouldn't achieve a thing if it wasn't for your guidance, values and love. I cannot thank you enough and I hope one day I can return back all you have done for me.

To Professor Carlos Leitão, Professor Sree Sabari and Professor Dulce Rodrigues, the supervisors of this thesis, for all the knowledge shared, encouragement and availability provided. Despite all the difficulties, your presence was always constant and always made me push forward.

To David Andrade, for all the answered questions and continuous help through all the steps of this investigation. The good environment at the laboratory along with your patience for all the clarifying was crucial during these last months.

To Ivan Galvão, for the suggestions that also contributed to the development of this work.

To all my friends from high school and university, especially to Rafael, Hugo, Vicente, Tiago, Meneses, Alcoforado, Nuno, Tomás, Manuel, Vladimir, Francisco and Sérgio, for all the adventures, laughs and tears of joy. Your friendship is gold.

Finally, to Maria, for being a pillar of trust, care, companionship, patience, and love during the daily challenges of life, a very special thank you.

An additional acknowledgement goes to FEDER funds for sponsoring the research where the subject of this dissertation is included, through Portugal 2020 (PT2020), by the Competitiveness and Internationalization Operational Program (COMPETE2020) and national funds through the Portuguese Foundation for Science and Technology, under the projects: UID/EMS/00285/2020, POCI-01-0145-FEDER-00763 and Friction 4.0 (POCI-01-0145-FEDER-032089).

Abstract

In the present dissertation, the influence of the Friction Stir Spot Welding (FSSW) process parameters on the torque and temperature evolution of aluminium alloys is evaluated. For this purpose, spot welds were made using tools with variable diameter and different rotational speeds. The base materials consisted of three heat treatable aluminium alloys (AA2017-T451, AA6082-T651, AA7075-T651) and one non-heat treatable aluminium alloy (AA5083-H111).

The temperature measurements were performed with the aid of a thermographic camera and the torque was recorded using the equipment where the welds were produced. The treatment of the process data allowed to compare the thermal cycles and the torque values for the different welding conditions tested.

The relationships between process parameters and outputs were established by adjusting an analytical model to the experimental results. The obtained equations were used to create 3D surfaces, which proved to be able to predict satisfactorily the evolution of both torque and temperature with the variation of the process parameters.

The developed work allowed to conclude that, for the FSSW process, tool dimensions and rotational speed have different influences on torque output and heat generation. More precisely, under the chosen process conditions, the shoulder diameter governed the heat generation while the rotational speed had a minor influence on the temperatures achieved. In addition, the torque output was largely affected by both the shoulder diameter and the rotational speed. The different material properties showed no effect on the torque and temperature values obtained.

Keywords FSSW, Aluminium, Torque, Temperature, Modelling

Resumo

A influência dos diferentes parâmetros de processo sobre o binário e a temperatura desenvolvidos em soldaduras produzidas por *Friction Stir Spot Welding* (FSSW) em diferentes ligas de alumínio, foi estudada na presente dissertação. Para tal, as soldaduras foram realizadas com recurso a ferramentas de vários diâmetros e usando diferentes velocidades de rotação. Como materiais de base foram utilizadas três ligas de alumínio tratáveis termicamente (AA2017-T451, AA6082-T651, AA7075-T651) e uma liga de alumínio não tratável termicamente (AA5083-H111).

As medições de temperatura foram realizadas com o auxílio de uma câmara termográfica e o binário foi registado através do equipamento onde foram produzidas as soldaduras. O processamento dos dados do processo permitiu comparar os ciclos térmicos e os valores do binário para as diferentes condições de soldadura testadas.

Relações entre os parâmetros e os *outputs* do processo foram estabelecidas ajustando um modelo analítico aos resultados experimentais. As equações obtidas foram usadas para criar superfícies em 3D, que se mostraram capazes de prever de um forma satisfatória a evolução, quer do binário, quer da temperatura com a variação dos parâmetros do processo.

O trabalho desenvolvido permitiu concluir que, para o processo FSSW, as dimensões da ferramenta e a velocidade de rotação influenciam, de forma diferente, a evolução do binário e o calor gerado. Mais precisamente, para as condições de processo estudadas, a dimensão da ferramenta governara a geração de calor, enquanto que a velocidade de rotação teve uma menor influência nas temperaturas alcançadas. A evolução do binário mostrou ser bastante influenciada pelo diâmetro da base da ferramenta e pela velocidade de rotação. As diferentes propriedades dos materiais não demonstraram qualquer influência nos valores de binário e temperatura obtidos.

Palavras-chave: FSSW, Alumínio, Binário, Temperatura, Modelação

Contents

LIST OF FIGURES

LIST OF TABLES

LIST OF SIMBOLS AND ACRONYMS/ ABBREVIATIONS

List of Symbols

C_M – Torque Coefficient

C_T – Temperature Coefficient

D_p – Pin Diameter

D_s – Shoulder Diameter

d_z – Plunge Depth

F_z – Axial Force

G – Geometry Parameter

J_2 – Second Invariant of Deviatoric Stress

M – Torque

M_{Man} – Maintenance Torque

M_{Max} – Maximum Torque

p_r –Plunge Rate

R^2 – Pearson Correlation Coefficient

t – Thickness

T –Temperature

T_{Man} – Maintenance Temperature

t_{man} – Maintenance Time

T_{Max} – Maximum Temperature

δ – Sticking Fraction

v – Transverse Speed

$\tau_{contact}$ –Contact Shear Stress

τ_{yield} – Yield Shear Strength

ω – Rotational Speed

Acronyms/Abbreviations

BM – Base Material

FSSW – Friction Stir Spot Welding

FSW – Friction Stir Welding

HAZ – Heat Affected Zone

PAZ – Process Affected Zone

RSW – Resistance Spot Welding

SZ – Stir Zone

TAFSW– Tool Assisted Friction Spot Welding

TAFW – Tool Assisted Friction Welding

TMAZ – Thermomechanically affected zone

TWI – The Welding Institute

1. INTRODUCTION

Friction stir welding (FSW) is a solid-state linear joining process, developed and patented in 1991, by Wayne Thomas at The Welding Institute (TWI). This joining technology, which welds reach about 80% of the base materials melting point, emerged with the objective of overcoming the difficulties of fusion welding, especially in aluminium alloys. Beyond producing welds with good mechanical properties, also, due to the reduced amount of heat generated, the FSW process allowed to minimize the occurrence of defects and distortions. The study and development of the technology permitted to extend the process functionalities to other welding variants and other materials beyond aluminium, such as steels and dissimilar materials. One of those variants, the Friction Stir Spot Welding (FSSW) process, is a spot joining technology based on the FSW operative principles, but without the traverse movement of the tool. With the increasing use of Aluminium alloys as an answer to the demand on vehicle weight reduction, FSSW quickly became a promising option to substitute fusion spot welding, Resistance Spot Welding (RSW) or the typical joining by riveting.

The main goal of any scientific study on joining processes is to develop its reproducibility and efficient application at the industrial level in which, high quality requirements must meet high volume production. In this context, the analysis and prediction of the thermomechanical responses during FSSW are of extreme relevance in order to optimize the process parameters selection.

In the present work, spot welds were produced using the FSSW technology, in singular 10 mm plates of different types of aluminium alloys, more specifically the heat treatable (AA2017-T451, AA6082-T651, AA7075-T651) and non-heat treatable alloys (AA5083-H111). Four different tools and rotational speeds were used. The thermal cycles were acquired through a thermographic camera and were associated with the output torque values registered through the welding machine. The obtained data was treated and further ahead analysed considering the different process parameters and the selected base materials. An analytical model was introduced to establish the relationships between the outputs and the process parameters. The obtained equations were used to create 3D surfaces, which proved to be able to predict in a satisfactory way the evolution of both torque and temperature, with the variation of the process parameters.

The present work is divided into 6 chapters. After an initial introduction in chapter 1, the state of the art is presented in chapter 2, where is conducted a literature review. The chapter starts describing the FSW technology along with the variants that surged with it. Afterwards, is carried a more focused review of the work already developed on the heat generation and torque output for the FSSW process. In chapter 3 is explained the experimental procedure, along with the tools used, the process input parameters, the base materials properties and some details about the data treatment. The analysis and discussion of the results are developed in chapter 4. In chapter 5 is introduced an analytical model, in order to predict the outputs' evolution for a broader range of parameters. Finally, in chapter 6 are presented the main conclusions of the present investigation as well as some recommendations for future work inside the same field of investigation.

2. STATE OF THE ART

The ability to permanently join two or more separate elements, from similar or dissimilar materials, was critical to take our world to the technological era we live in. Present in a wide range of highly important industries, even though passing unnoticed in daily applications, it's safe to say that welding keeps our world together.

Welding technologies can be separated in two main branches: Fusion welding processes, in which the materials to be joined reach temperatures above their melting temperature, and solid-state welding process, in which the temperatures reached do not exceed the base materials melting temperature.

This chapter begins by presenting a specific solid-state welding process, called Friction Stir Welding (FSW), and follows with the description of some of its main progress and related technologies, one of which, the Friction Stir Spot Welding (FSSW) technology, which was the motivation for the present dissertation. The chapter is finalized with a review on the work already developed on the study of the heat generation in FSSW and on process control by torque sensitivity analysis.

2.1. Friction Stir Welding (FSW)

Friction stir welding is a solid-state joining process developed and patented by The Welding Institute, Abbington UK, in 1991, with the objective of overcoming the difficulties associated to the fusion welding of aluminium alloys[1]. The process quickly brought numerous advantages such as the possibility of joining "non-weldable" aluminium alloys, in similar and dissimilar combinations, while providing satisfactory joint strength and eliminating fusion welding related defects, like porosities, shrinkage or hot cracking. This technology is also classified as a "green" process, due to the absence of filler metals, fluxes, spatter or shielding gases, together with an high efficiency in energy usage[2][3]. For these reasons, over the last three decades, the FSW technology has been under constant study and development, becoming a core process in the Aerospace, Railway, Automotive, Electronic and Shipbuilding sectors [4]. The literature review enables to identify many technologies related or emerging from the FSW process, which has more than 3000 new patents published since 1993, all over the world [4]. These FSW variants present changes

to the conventional process practices, in order to solve some technological existent problems or to enhance the performance of the process.

A schematic example of the conventional FSW process is illustrated in Figure 2.1. As shown in the figure, the process begins with a non-consumable rotating tool, usually constituted by a cylindrical shoulder with an embedded pin, being plunged into the interface of the components to be joined. Once the shoulder reaches the top surface of the workpiece, both the pin and the shoulder start promoting heat generation by friction. As the temperature rises, the material softens, without ever reaching its melting point. However, as result of the softening, the tool is able to stir the material, by plastic deformation, around the pin and under the shoulder. After this stage, the thermo-mechanical conditions stabilize and the tool starts moving linearly with a controlled traverse speed, until the weld is completed and the tool is retracted. At the end of the weld, an exit hole (keyhole) is created, as a result of the pin insertion into the interface [2][5].

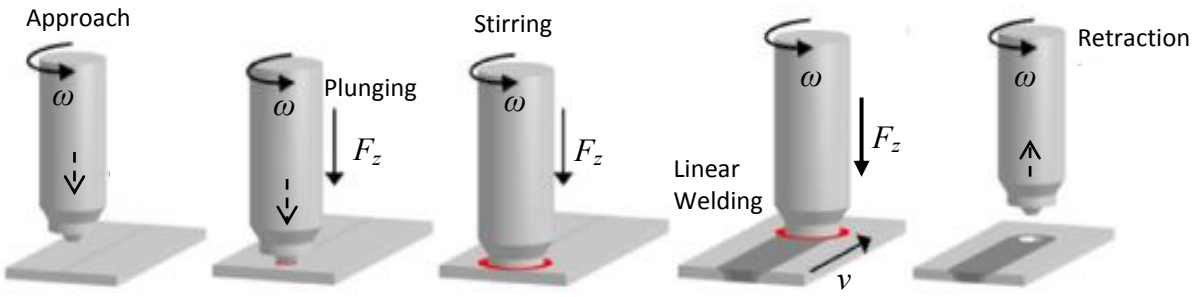

Figure 2.1 Schematic representation of the FSW process (adapted [2]).

In the scheme of Figure 2.1 are also represented the main process parameters for FSW, i.e., the tool rotational (ω) and traverse (v) speeds, and the axial force (F_z), which affect the amount of heat generated by friction and plastic deformation, due to contact conditions and mixing of the base materials during the process [2][6][7]. Changing the shoulder or the pin size and geometry is also a major factor influencing heat input, the stirred material volume and its flow patterns, affecting directly the weld quality and morphology [5][8].

In Figure 2.2 is shown some of the existing pin/shoulder configurations. With the purpose of eliminating the keyhole, pinless tools started to be used along with grooved profiles on the shoulder surface's (Figure 2.2 b). The improvement of using these tools'

geometry, was reported by some authors, who observed that the pinless tools were able to attain higher service life and, in certain variants of the process, these tools could even attain similar or increased welding strength when compared to the tools with an embedded pin [9][10][11][12].

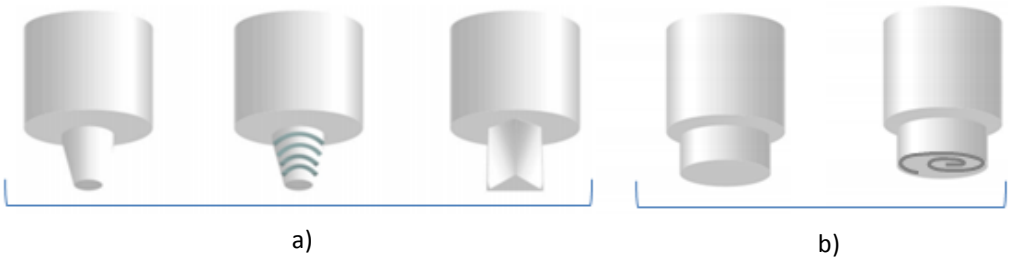

Figure 2.2 FSW tool geometries a) FSW tools with different pin geometries and features, b) FSW pinless tools (flat shoulder and scroll profiled shoulder) (adapted [12]).

One worth naming FSW related technology, that makes use of a pinless tool, is the Tool Assisted Friction Welding (TAFW). This technology was created at the University of Coimbra, and was initially developed for the linear lap joining of thin steel plates using a pinless tool with a flat and featureless shoulder [9]. While in FSW, the tool pin promotes the joining by the stirring of the base materials across the abutting interface to be connected, in TAFW, the tool characteristics lead to a distinctive joining mechanism. More precisely, due to the pin absence, in this variant, there is no stirring of the base materials across the interface to be bonded, being the connection obtained through a combination of plastic deformation and high temperature atomic diffusion, comparable to that occurring in forging and friction welding processes.

Another FSW related technology with increasing importance is the Friction Stir Spot Welding (FSSW) process, a technology based on the same concepts of the FSW but adapted to the production of spot welds. Detailed information on the FSSW process operation, its applications, the involved parameters and how they affect heat generation and torque output, will be presented in the following section.

2.2. Friction Stir Spot Welding (FSSW)

The FSSW technology is based on the same operative principles of the FSW process, however, since the production of spot welds is envisaged, the linear translation of the tool is suppressed and, instead of the traverse speed, the welding time becomes one of the most important parameters of the process. In spite of this, the FSSW technology offers the same metallurgical, environmental and energy benefits of the original FSW process when compared to other spot joining techniques.

The typical daily cars contain between 2000 to 5000 spot welds, meant to join most of the overlapping sheets in its structure. With the increasing use of aluminium alloys, for reducing the vehicles' weight, the FSSW technology quickly became a promising option to substitute the traditional Resistance Spot Welding (RSW) process, fusion spot welding or the typical joining by riveting [13]. An example of the process application in the automotive industry can be observed in Figure 2.3 [14].

Over the last decades, many modifications to the traditional FSSW procedures have been proposed, being the two more intensely investigated variants of the process, the Pinless FSSW [10] and the Refill FSSW [15]. Even though many progress has been achieved, in order to extend the FSSW industrial applicability, it is valuable to have a structured analysis of the process mechanisms, such as the heat generation, material flow, welding parameters, tool design, microstructure evolution and mechanical properties[16]. On the following sections, only the conventional FSSW process and its Pinless counterpart will be discussed.

Figure 2.3 FSSW industrial application in Mazda Motor Corp.[14].

2.2.1. Conventional FSSW

The typical FSSW technique can be divided in three stages as shown in Figure 2.4 [17]. As is sketched in the figure, the rotating tool, with a coupled pin, plunges at a pre-established rate (Figure 2.4 a), into the plates, until the shoulder reaches a predefined depth. In FSSW related terminology, the rate at which the tool descends into the workpiece is the plunge rate (p_r) while the distance that the shoulder penetrates into the workpiece is labelled as plunge depth (d_z). As in FSW, the mechanical interaction between the tool and the plates promotes frictional heating, which softens the base material. To sustain the tool downward force, applied on the workpiece during the process, an anvil, or backing plate, is used on the bottom of the workpiece. The dwell stage (Figure 2.4 b) begins after the plunge depth is achieved, and remains for a pre-defined period of time, normally a few seconds, during which the tool promotes the mixing of the two different sheets, creating a solid-state joint. The amount of time that the tool remains plunged at this stage is defined as the dwell time or maintenance time (t_{man}). After this period, the tool retracts (Figure2.4 c), leaving an undesirable keyhole that significantly decreases the weld strength by acting as a stress concentration defect. The hole left by the tool is also a place prone to the occurrence of corrosion [18] [19].

The FSSW is a delusive simple process since the tool interactions with the base material are more complex than they first appear to be, which results from the highly transient welding conditions, as opposed to the original FSW, in which a steady state is achieved after the initial plunging and dwell periods.

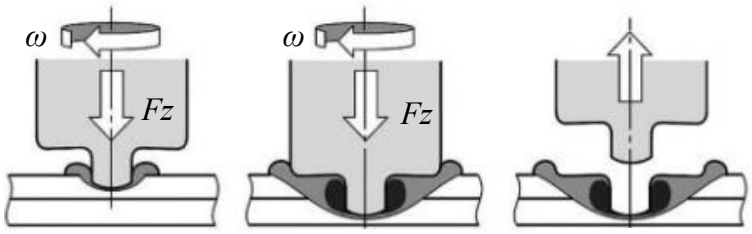

Figure 2.4 Conventional FSSW process stages a) Plunging, b) Dwell, c) Retraction (adapted [17]).

A cross-section of a conventional FSSW weld is shown in Figure 2.4 [20]. Analysing the image, it is possible to depict the region where the interaction between the tool and the plates took place and also the different heat affected zones associated to the process. The welds created by the conventional FSSW technique can be subdivided into

several regions, such as the stir zone (SZ), the thermomechanically affected zone (TMAZ) and the heat-affected zone (HAZ). There is also a portion of base material (BM) that is unaffected by the process. The SZ results from the intense plastic deformation and frictional heating promoted by the tool, being characterized by a fine equiaxed grained microstructure resulting from dynamic recrystallization. The TMAZ, on the other hand, is a region which experiences both deformation and temperature effects, but with less intensity than the SZ. As a result of this, recrystallization does not occur in this zone, which displays grains distorted and aligned with the stirring direction. Finally, the HAZ, is constituted by the portion of material that is not plastically deformed but goes through the process thermal cycle, reaching temperatures lower than the ones attainted in the TMAZ [21].

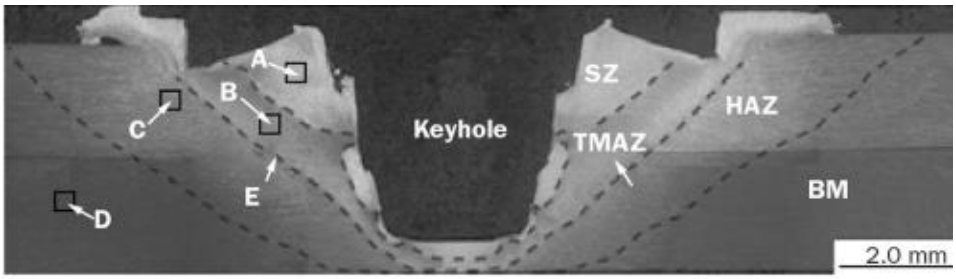

Figure 2.5 Weld zones in conventional FSSW [20].

Beyond the microstructure of the different weld zones, the post-weld hardness distribution in friction spot welds is also conditioned by the differences in the chemical and metallurgical structures of the alloy groups as well as on the applied strengthening mechanisms, also referred as tempers.

Depending on the intensity and duration of the thermal cycle, for some heat treatable alloys, the welding process may act as an additional heat treatment for the HAZ. Generally, heat treatable aluminium alloys tend to obtain more softened HAZ's due to coarsening or dissolution of strengthening precipitates during the process thermal cycle.

Non-heat treatable alloys are strengthened through cold working, thus, in most of the cases, the FSSW process can lead to an increase of the hardness in the SZ and in the TMAZ due to the additional plastic deformation, on the other hand, the HAZ is generally annealed losing the tempering effect [16].

For this reason, the study of the thermal cycles during the FSSW process is of important relevance.

2.2.1.1. Heat Generation in Conventional FSSW

The peak temperatures reached in conventional FSSW, which range from 0.94 to 0.98 of the solidus temperature of the base material [22], have a strong influence on the final joint strength and weld microstructure. Thus, understanding and predicting the thermal cycles, i.e., the evolution of the temperature with time, is crucial to optimize the welds mechanical properties, thus increasing the technology potential.

The literature on FSSW enables to identify two main sources of heat generation during the process. The heat generation due to friction at the tool/workpiece interface (surface heat source), already identified in this Introduction, and the heat generation due to the plastic deformation, associated to the base materials stirring (volume heat source).

Some authors purposed models that assume the surface heat source as the main source of heat generation, representing about 97% of the total energy, while the volumetric heat source is just about 3% of that energy [23].

In contrast, other works showed that the volume heat source has a considerable effect on the prediction of the maximum temperatures reached [24] and that 95% of the mechanical input power, that is turned into plastic deformation energy, is converted into heat, while the rest of it is stored in form of defects and in the grain boundaries. The volume heat source is usually related to the amount of plastic work converted into heat (β), the plastic strain rate ($\dot{\varepsilon}$) and the Cauchy stress tensor (σ_{ij}) [25].

The heat sources previously referred, are directly dependant on the interface contact conditions and, for that reason, the ratio (δ) between the workpiece contact surface velocity and the tool's contact surface velocity is used to define sliding, sticking or partial sliding-sticking conditions. Sliding contact conditions (δ=0) are attained when the contact shear stress is lower than the alloy matrix yield shear stress (τ_{yield}), corresponding to pure friction heating. Sticking contact conditions (δ=1), on the other hand, occur when the contact shear stress surpasses the yield shear stress (τ_{yield}) of the base material, and, in that scenario, the softer material sticks to the tool's moving surface. So, when sticking contact prevails, the heat is mainly generated by the plastic deformation of the base material. Partial sliding-sticking conditions are a mix of both phenomena's ($0<\delta<1$), in this case, both the surface friction and plastic deformation are considered to contribute at the same time for heat generation. Actually, during the FSSW process, with the temperature changing in space and time, yield shear stress values are not constant, implying that the

contact conditions may also vary both spatially and temporally. This is the reason why it is frequently unclear to know in reality the contact conditions that prevail during FSSW [26].

When it comes to the process parameters, the ones reported in the literature as having the major influence on heat generation are the tool geometry (pin and shoulder dimensions/features), the tool rotational speed, the dwell time and the plunge rate. The right combination of these parameters is essential to produce good quality welds, since they must provide enough energy to create the metallurgical bonding while reckoning that an excessive heat input can lead to defects that reduce the strength of the welds [27].

Considering the tool geometry, an experimental work was conducted using the AA6111-T4 alloy in order to understand the effect of different pin lengths on the welds' quality under the same process conditions. It was demonstrated that increasing the pin length from 0.7 to 1.6 mm, resulted in an increase in the peak temperature of about 50ºC [19]. Besides the pin length, the heat generated during welding is also proportional to the shoulder diameter, due to the expansion of the frictional contact area [26].

The heating rate input is also strongly associated with the rotational speed [28]. A study regarding conventional FSSW, conducted on the AA7075-T6 thin sheet, showed that by changing the rotational speed from 1000 rpm to 3000 rpm increased the heating rate from 275 ºC/s to 400 ºC/s and the maximum temperatures from 440 ºC to 527 ºC, while considering a dwell time of only 4 seconds. Yet, on the same study, after a stabilization period (~10 seconds of dwell time), independently from the rotational speed, extrapolated temperature values tended to approach to the same limit value. The peak temperatures, achieved at the stir zone, were found to be limited by the base material solidus temperature or by transient local melting of second phase particles, which can also be responsible for temperature fluctuations during the process [22]. A thin film of melted material at the contact interface, between the tool and the workpiece, has a lower viscosity than regular plasticized material, this causes the tool to slip, decreasing the strain rate and heating rate. The liquid films will slowly solidify, raising the viscosity and the temperature once again. This local melting effect is not always attainable during the FSSW process and is strongly dependent on the welding parameters that affect the amount of heat input necessary to reach that state [28][29].

Increasing the plunge rate is convenient for time-saving purposes, conferring a productivity advantage. This parameter determines how fast the workpiece will face thermomechanical changes. A numerical simulation work showed that by decreasing the plunge rate, from 10 mm/s to 1 mm/s, the frictional heat dissipation energy increased about 86% and the plastic dissipation energy increased about 60% [23]. In the same way, an experimental study, conducted on the AA6061-T6 alloy at 3000 rpm, concluded that by decreasing the plunge rate from 5 mm/s to 0.1 mm/s resulted in an absolute increase of the total energy generated of 32.18 kJ [29]. Essentially, the slower the plunge rate, the more time the tool will be spinning on the workpiece until it reaches the predefined depth, thus more energy is produced. However, this concept is more prominent for shorter dwell times, given that peak temperatures will be insensitive to plunge rate as the total processing time increases.

The dwell time is a key parameter to ensure the necessary energy input to form the stir zone and create a bonded region between the two sheets. Higher dwell times conduct to higher temperatures attained, until a certain limit, since the process converges to a thermal balance through self-stabilizing conditions. Increasing this parameter will allow converting more mechanical energy into heat, not only due to the increase in total welding time but also because of shoulder contribution to heat generation that begins at this stage. An experimental work concluded that, for the first dwell time seconds, about 70% of the energy generated is produced by the pin, but if the dwell period holds for over 4 seconds, the shoulder contribution to heat generation can markedly increase to about 50% [30]. Widening of the softened region in the HAZ, was also reported to be associated with higher dwell time periods in heat treatable aluminium alloys [31].

Despite not being considered a process parameter, the materials used for the anvil and clamping also have an influence on the heat accumulation during the process. When subjected to the same process conditions, when using a ceramic anvil and clamps about 50% of the energy applied is transferred into the workpiece while, if using a steel anvil and clamping, only 12.6% of the same energy is transferred into the workpiece. With more energy being transferred to the sheets through the usage of ceramic parts, the softened HAZ becomes larger than the one using steel parts [29][30].

Besides experimental research, another way of analysing and predicting the thermo-mechanical response of the materials in FSSW is trough modelling. Unlike FSW, the spot joining technique is a transient process when it comes to material flow,

temperature distribution and contact/friction conditions, making the analytical or numerical modeling work much more complex.

An Analytical model recognizes parameters from different geometrical, energetic, and physical possibilities, and correlates their dependencies empirically through algebraic expressions to estimate heat generation [32]. In figure 2.6 are graphically represented the relationship between some of the parameters that can influence heat generation in FSSW. For instance, the contact shear stress, $\tau_{contact}$ in the figure, is dependant but at the same time influent on the contact conditions (δ), the friction coefficient (μ), the torque (T in the figure) and in the heat generation (Q_t). Other parameters such as the rotational speed (ω), the tool geometry, the pressure (p) and the yield shear strength τ_{yield} are also directly or indirectly correlated.

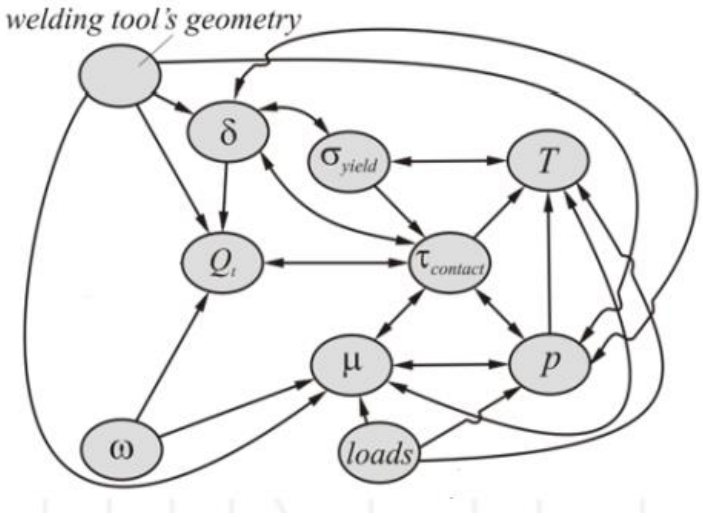

Figure 2.6 Graphical representation of the relationship between influencing parameters (adapted [32])

Computational tools are also used as a way to simulate and visualize the influence of different process conditions on heat generation, material flow and stresses involved during the FSSW process. Nowadays, FSSW can rely on different software, that allows the setting of different mesh geometries, temperature control equations, boundary conditions, contact conditions and material equations to create 2D or 3D FE thermo-mechanical models, replicating experimental results with high precision [16][33].

2.2.2. Pinless FSSW

With a simpler design, but based on the same operative principles of FSSW, Pinless FSSW emerged as a way to overcome the keyhole defect associated to the conventional process [16]. Beyond removing the stress concentration factor of the keyhole, the new process showed that it could attain comparable or even superior joint integrity, with higher failure energies, since it also proved to reduce the hooking defect. This largely reported defect is associated to the upward flow of the bottom sheet material and oxide particles that create an unbounded region with a hook shape [34]. Other considerable advantages is that the process demonstrated to be especially suitable for thin sheet applications, since the depth of indentation is reduced, and it also allowed to maximize the tool's service life turning the technology even more efficient [10][19].

Just as conventional FSSW, the tool rotational speed, the plunge rate, the plunge depth and the dwell time continue to have a significant impact on heat input and material flow. In this variant specifically, the interaction between the tool and the material fully occurs at the shoulder interface, hence, the shoulder dimensions and its surface features are crucial in heat generation and material flow [10][35].

When applying a pinless tool with a flat and featureless shoulder, the spot joining process is also denominated Tool Assisted Friction Spot Welding (TAFSW). The bonding mechanism results mostly in a combination of forging pressure and frictional heating that promote atomic diffusion, instead of major plastic intermixing of materials. A scientific article report based on TAFSW applied on the lap welding of steels, concluded that under certain conditions, there was no mixture of the base materials through plastic deformation and that the interface between the sheets was still visible after the welding process[36].

Most of the research done up to date focuses mainly on the effect of the process parameters on the microstructure and on the mechanical strength of the welded joints. A lack of development remains when it comes to heat generation and torque output as a control parameter, more even if considering specifically pinless FSSW.

2.2.2.1. Heat Generation in Pinless FSSW

Most of the concepts developed for the heat generation in conventional FSSW can be applied to the pinless variant.

One of the first researches performed on pinless FSSW showed the relevance of the shoulder profile on the maximum temperatures attained during the welding and on the material flow. The tests were conducted on AA6111-T4 aluminium alloys, using a rotational speed of 2000 rpm and a dwell time of 2.5 seconds. The authors report that when using a 10 mm flat and featureless shoulder, the maximum temperature obtained was of 380ºC while when using a fluted wiper surface shoulder, the maximum temperature reached around 430ºC [37]. The shoulder diameter was also reported to be directly proportional to the maximum temperatures registered and to the heating rate input [38].

An experimental work, conducted on the AA6061 aluminium alloy, identified the dwell time and plunge depth as being highly significant parameters influencing the temperatures attained in pinless FSSW [39]. For a scrolled pinless tool, changing the dwell time from 3 to 5 seconds, caused the temperature to increase from 267.82 ºC to 305.68 ºC at 1000 rpm and from 274.35 ºC to 309.9 ºC when using 1500 rpm. It was also observed that an absolute increase of the plunge depth values in just 0.05 mm, resulted in the increase of the registered temperatures of about 30 ºC [39]. It was concluded that increasing the plunge depth would result in an increase of the contact area responsible for heat generation. In the same work, it was reported that by changing the tool rotational speed from 750 to 1250 and then to 1750 rpm, the obtained changes in temperature were of about 0.01 ºC/rpm, which describe an almost negligible effect of the rotational speed in the heat generation [39].

Through a numerical simulation conducted on the AA2198-T8 aluminium alloy, welded at 950 rpm, with a 15 mm diameter pinless scrolled tool, the authors could observe the dynamic evolution of the temperature fields throughout the dwell stage as shown in Figure 2.7. The highest temperatures were developed beyond 2/3 of the shoulder radius, as a result of the radial velocity of the tool surface that linearly increases from zero at the centre, to a maximum value at the shoulder periphery. It is also possible to observe the decreasing temperature gradient between the sheets during the dwell stage, demonstrating once again the non-steady state characteristic of the process [40].

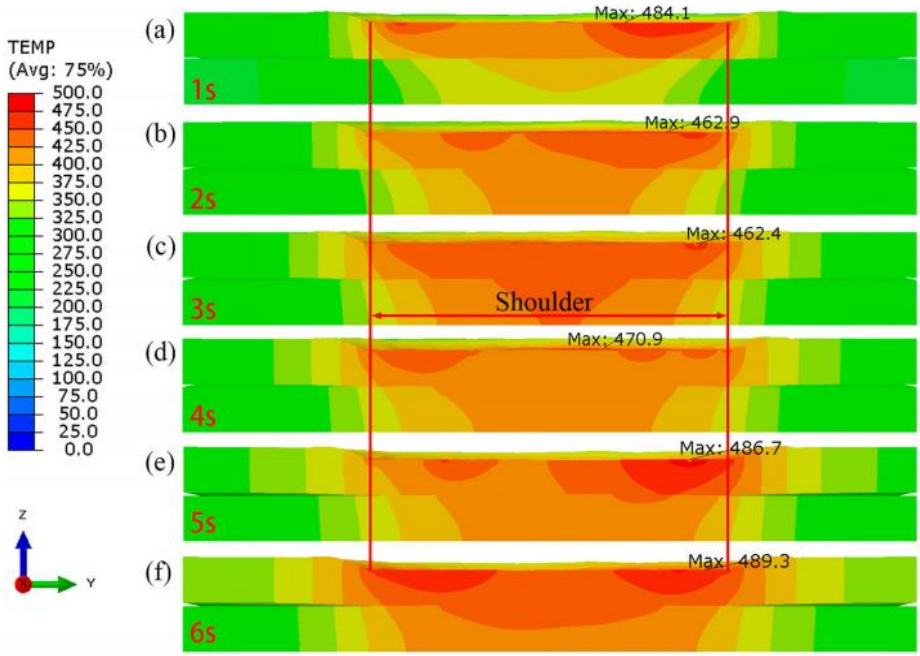

Figure 2.7 Simulated temperature distribution of pinless FSSW during dwell stage (adapted [40]).

2.2.3. Thermomechanical conditions in FSSW

The axial force was initially used a way to the control of the FSW process, yet it proved to have a non-linear relationship with many of the process parameters. Later, the torque output signal was found to be relatable to a wider the range of processing variables suitable for a stable control of the process, allowing to produce welds without defects. Additionally, the different thermomechanical phenomena that occur during the welding could also be associated with this output [6][8][36][41]. In FSSW, the spindle torque has also been recently used as a real-time monitoring instrument for overall process control. Hence, understanding and modelling the influence of the different process parameters on the torque has great potential for the development of this spot welding technology [27].

The typical torque evolution during the FSSW process is widely reported and is better illustrated in figure 2.8 [19]. During the initial plunging stage, the sudden changes in contact conditions cause a rapid increase in the torque values and a peak is achieved when the tool reaches the plunge depth. The curve then falls off when the dwell stage begins, as the material softens through heating, reducing the effort needed to stir the material around the tool. Meanwhile in conventional FSSW, due to the pin, the contact surface increases progressively as the tool penetrates into the workpiece, in pinless FSSW, the shoulder surface interacts with the material more abruptly, resulting in a sharper torque

peak. Despite this, since the overall contact surface is smaller, the average torque during the dwell stage is lower than the one obtained with a conventional tool [19]. Also, the heat accumulation caused by using an insulating anvil (made of ceramic material for instance), results in the decrease of torque, since the stress necessary to shear the material is inversely proportional to the increase temperature.

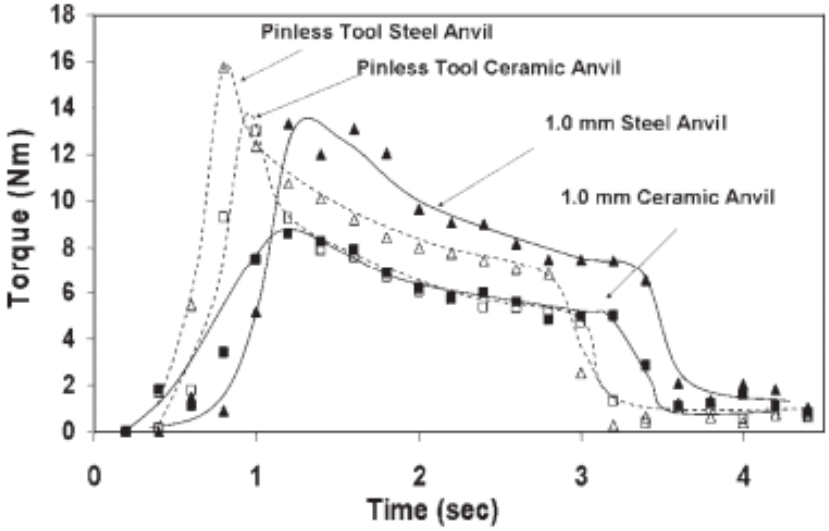

Figure 2.8 Torque curves for different pins and different anvils [19].

Larger tool dimensions are also reported to increase the torque output. Since the welding torque is the sum of all infinitesimal torques acting along the tool/workpiece contact surface, larger contact areas will provide higher torque values. This can be obtained by increasing the shoulder diameter, the pin length or even the plunge depth [27].

The torque output during the FSSW process is known for being inversely proportional to the rotational speed, meaning that by using higher rotational speeds, lower torque values are expected, as shown in Figure 2.9. The cause of this phenomenon is associated with the increase in heat input when the rotational speed is amplified. Due to this, the material softens, inducing less stress on the tool, resulting in a smaller torque output [31]. An experimental study, using a tool with a 2.2 mm pin and a 10 mm shoulder, conducted on the AA6061-T6 alloy, registered a decrease in torque from 15 to 5 N.m when spot welding at 1000 and 3000 rpm respectively [30].

In a different article, now conducted on the AA5754 alloy, with a scrolled flat 18 mm shoulder, the registered maximum torque values ranged from 58 to 19 N.m, with

the rotational speeds varying from 988 to 3511 rpm [42]. In addition, on the same work, it was also concluded that with higher plunge rates, the toque also increased at higher rates.

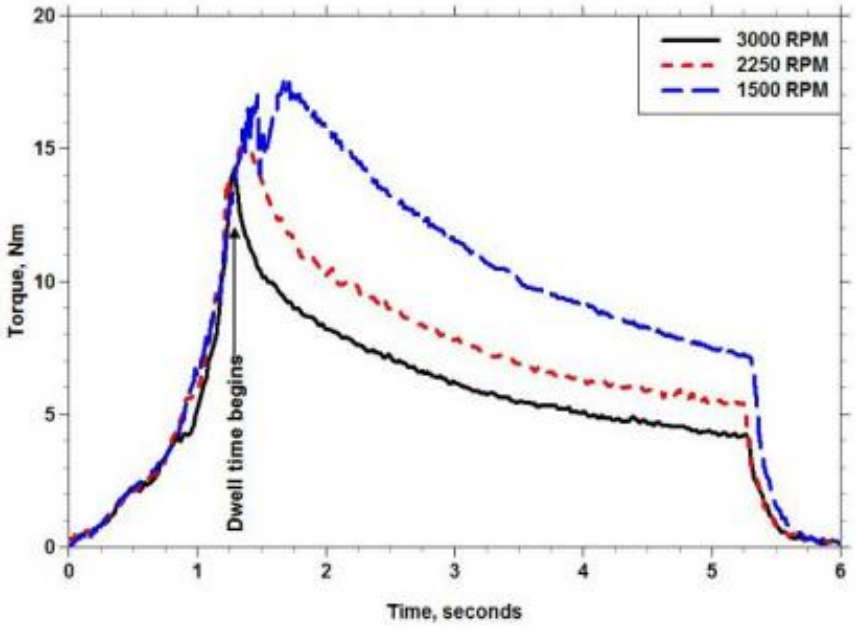

Figure 2.9 Effect of rotational speed on Torque [32].

The works described shown the high relevance of having an analysis and a prediction of the thermomechanical responses during a certain friction-based technological process, per instance, in order to optimize the process parameters. In this context, in present work, the torque output and the thermal cycles, obtained during Pinless FSSW, are analysed considering different welding conditions for several aluminium alloys. Strong process input/output relationships were determined and an analytical model is introduced, in order to predict the thermomechanical response of the process and to perform a deeper analysis of the thermomechanical phenomena occurring during the process.

3. EXPERIMENTAL PROCEDURE

In this work, about ninety-five spot welding operations were simulated using different aluminium alloy plates, with 10x10 cm width and 10 mm thickness, of the AA2017, AA5083, AA6082 and AA7075 aluminium alloys.

In Figure 3.1 [35] is shown the layout of the necessary elements to perform the welding simulations. All the tests were performed using an MTS 1-STIR PDS FSW machine. Previously to the welding tests, the samples were cleaned so that oil, rust and corrosion particles would not interfere chemically or mechanically with the welding operation. Due to the multi-axial forces and vibrations developed during the welding, rigid clamping was used alongside a steel anvil. All tests were done under position control and, as in real FSSW operations, their execution was divided in three stages (plunging, dwell and retraction), with a total duration time of 64 seconds. More details will be presented in this chapter. After the process, the samples were left to cool down at room temperature.

The influence of the base materials properties, tool dimensions and rotational speed on heat generation and torque output was assessed by varying each of these parameters independently, one at a time.

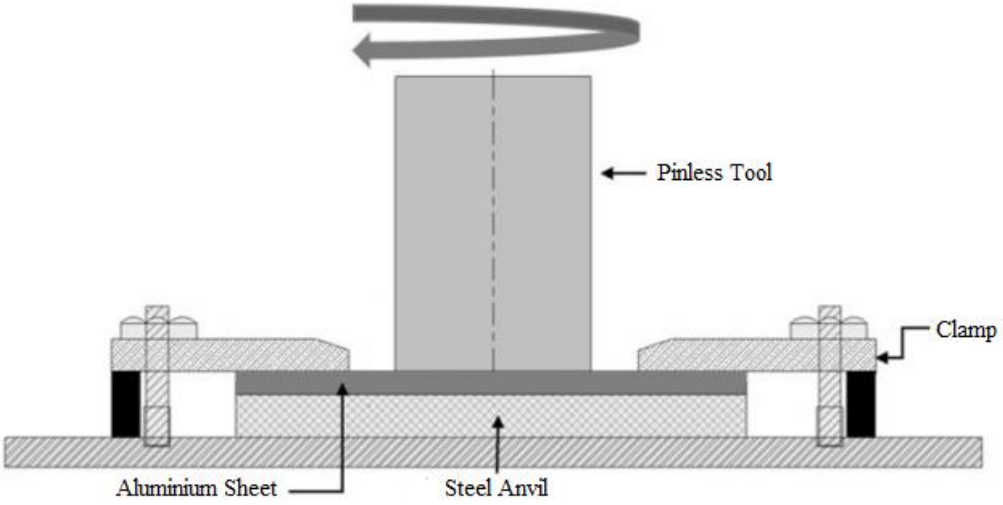

Figure 3.1 Schematic illustration of the experimental procedure (adapted [35]).

3.1. Base Materials

Four different aluminium alloys were used as base material, namely the AA2017, AA5083, AA6082 and AA7075. The AA2xxx alloy series are Al-Cu heat treatable aluminium alloys (copper addition of 0.7 - 6.8 %) with high strength and performance, being often used in aerospace and aircraft applications. The AA5xxx alloy series are Al-Mg non-heat treatable aluminium alloys, (magnesium addition of 0.2 - 6.2%), easily weldable, and for that reason often used in applications such as transportation, pressure vessels and shipbuilding. The AA6xxx alloy series are Al-Mg-Si heat treatable aluminium alloys (magnesium-silicon addition of ~1%) mainly used for structural components. Finally, the AA7xxx alloy series are Al-Zn heat treatable aluminium alloys (zinc addition of 0.8 – 12%) which compromises some of the highest strength alloys being commonly used in high-performance applications.

Differences in the chemical and metallurgical structures between the alloy groups have an important impact on heat generation and material flow during the welding process. In Table 3.1 is represented the chemical composition of the base materials, obtained from the supplier's technical sheet [43], and in Table 3.2 are summarized some mechanical and thermal properties, obtained from Aerospace Specification Metals (ASM) [44].

In the current work, considering the heat treatable alloys, the AA2017 alloy has a T451 temper while the AA6082 and the AA7075 alloys both have a T651 temper. Regarding the non-heat treatable alloys, the AA5083 alloy has a H111 temper. The temper designation and meaning corresponding to each alloy series is highlighted in table 3.3.

Table 3.1 Base materials chemical composition (maximum weight %) [43].

	Si	*Fe*	*Cu*	*Mn*	*Mg*	*Cr*	*Zn*	*Ti*
AA2017	0.2 - 0.8	0.7	3.5 - 4.5	0.4 - 1	0.4 - 1	0.1	0.25	0.25
AA5083	0.4	0.4	0.1	0.4 - 1	4 - 4.9	0.05 - 0.25	0.25	0.15
AA6082	0.7 - 1.3	0.5	0.1	0.4 - 1	0.6 - 1.2	0.25	0.2	0.1
AA7075	0.4	0.5	1.2 - 2	0.3	2.1 - 2.9	0.18 - 0.28	5.1 - 6.1	0.2

Table 3.2 Base Materials physical, mechanical and thermal properties [44].

Aluminium Alloy	*Density [g/cm^3]*	*Ultimate Tensile Strength [MPa]*	*Shear Strength [MPa]*	*Hardness [Brinell]*	*Thermal Conductivity [W/m.K]*	*Melting Point [ºC]*
2017-T451	2.78	427	262	105	135	513 – 640.6
5083-H111	2.66	275	172	75	117	590.6 - 638
6082-T651	2.70	340	210	98	170	555
7075-T651	2.81	540	331	150	130	477 - 635

Table 3.3 Temper Designation and Meaning.

Non-Heat Treatable	H111- Strain Hardened
Heat Treatable	T451- Solution heat-treated, stress relieved and then naturally aged. T651- Solution heat-treated, stress relieved by stretching and then artificially aged

3.2. Tools

Four different pinless tools, with a flat and featureless shoulder, were used to perform the spot welds, similarly to the FSSW process. The tools were all made from Tungsten Carbide, known for performing well at elevated temperatures, due to its high wear resistance and reasonable fracture toughness. The shoulder diameter (D_s) was the characteristic that differed between the tools being used, tools with 10, 12, 16 and 18 mm diameters. In the next, each tool will be labelled according to the shoulder diameter as PL10, PL12, PL16, and PL18, respectively.

In figure 3.2, where the different tools used to perform the spot welding tests are represented, shows that meanwhile the PL10 and PL12 tools consisted of a shoulder coupled to a modular body, the PL16 and PL18 tools were a compact single body tool, with a tapered geometry.

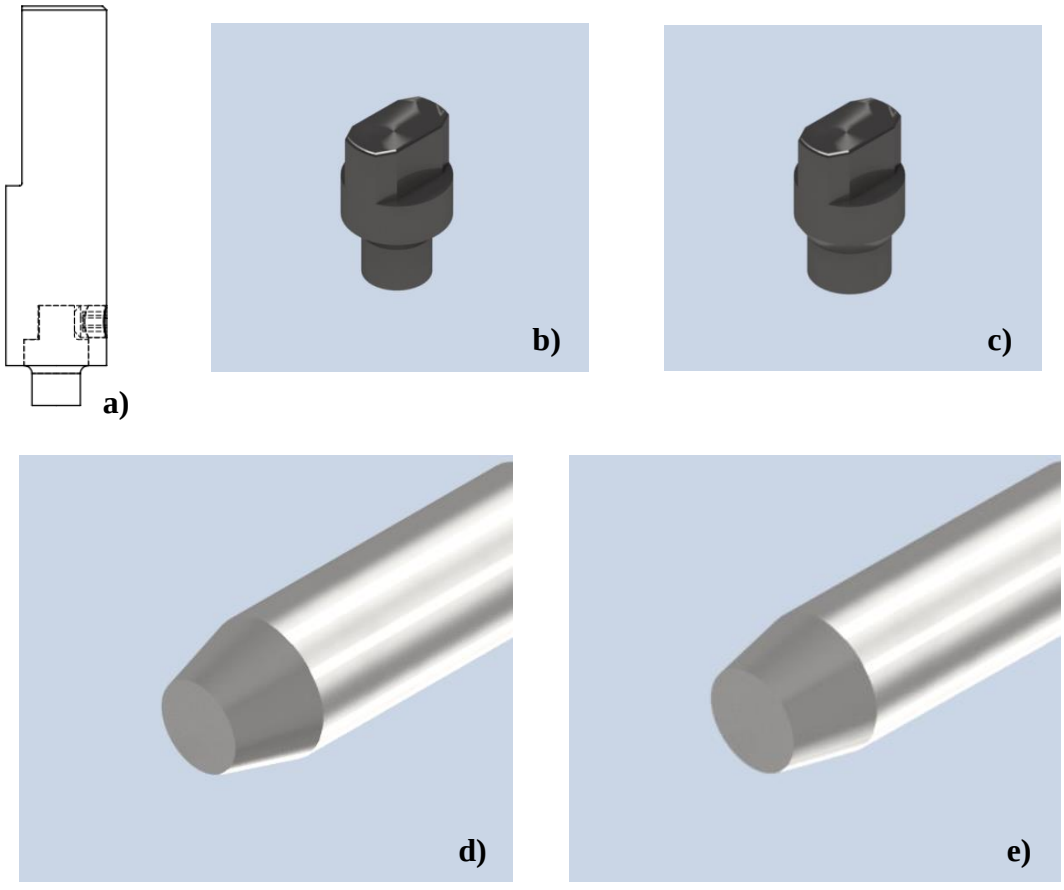

Figure 3.2 a) Modular tool b) PL10 and c) PL12 modules, d) PL16 and e) PL18 rigid body tools.

3.3. Process Input Parameters

As in FSSW, for the execution of the spot welding simulations, the processing variables were the tool rotational speed (ω), the shoulder plunge depth (d_z), the plunge rate (p_r), and the dwell holding time, also designated maintenance time (t_{man}). The machine positioning input parameters are graphically represented in Figure 3.3.

The plunge depth, which is the distance that the shoulder penetrates into the plates, was set to be constant for all the trials, with a value of 0.5 mm, representing 5% of the total plate thickness. The plunge rate, which represents the speed at which the tool descends into the plate until it reaches the plunge depth, was also kept constant through all the trials with a value of 0.125 mm/s, meaning that the whole plunging stage had a duration of 4 seconds. The dwell time was set to be 60 seconds for all the tests, making a total duration of 64 seconds for the execution of a single spot. Four different rotational speeds were used: 660, 870, 1140 and 1500 rpm.

It is important to enhance that these parameters were chosen, not to reproduce industrial process conditions, characterized by short welding times, but to be able to capture the differences in heat generation and temperature evolution between the different welding conditions.

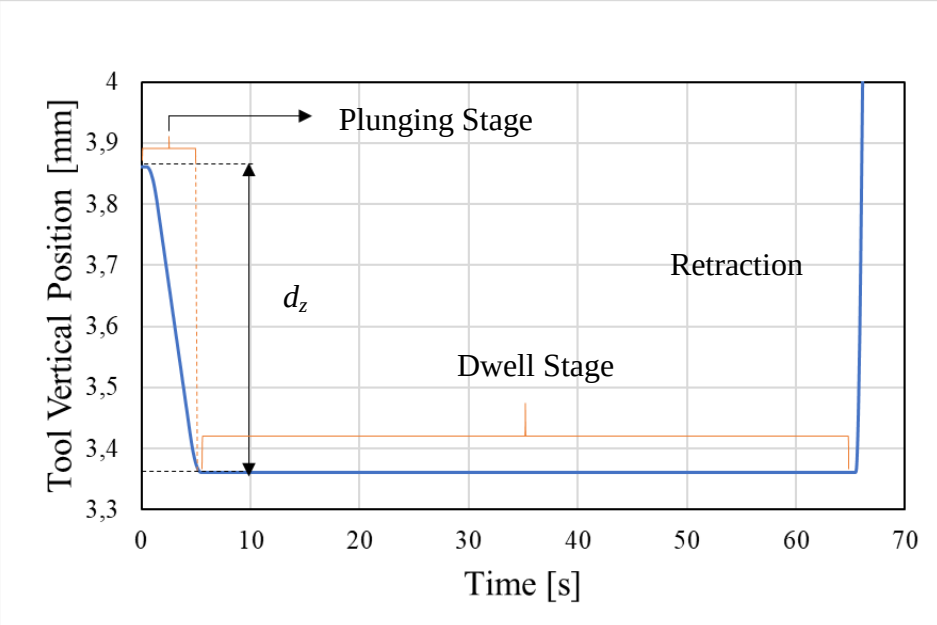

Figure 3.3 Evolution of the tool vertical position with time.

3.4. Temperature Acquisition

The temperature measurements were made with a "*FLIR A655sc*" thermographic camera, and its assembly was done as is shown in figure 3.4. The camera was mounted 0.3 m away from the welding spot, with the optic focused on the contact interface between the tool and the base material. The temperature was acquired using a 12.5 Hz frequency and an emissivity value of 0.95.

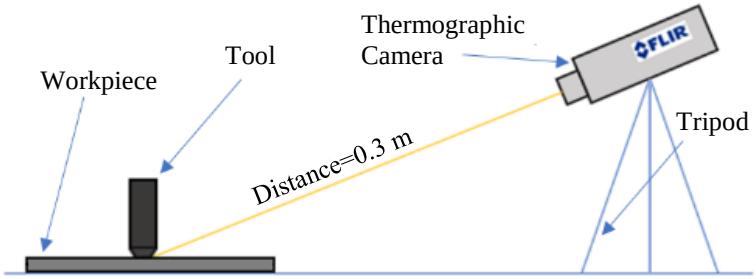

Figure 3.4 Schematic representation of the apparatus for temperature acquisition.

The graph in Figure 3.5 is an example of the treated temperature data associated to one spot weld. In order identify the different phases of the welding thermal cycles, i.e, the heating, stabilization and cooling periods, an instantaneous temperature related to time derivative (*dT/dt*) was calculated, after eliminating the noise associated to the raw acquisition data through a smoothing LOESS functionality, also known as Savitsky-Golay filter. Positive *dT/dt* values imply temperature rising (heating) and negative *dT/dt* value implies temperature decreasing (cooling). If there is no temperature variation, *dT/dt* approaches to zero (maintenance). Due to experimental reasons, the interval chosen to consider no temperature variation was *dT/dt* = [-4,4], which represents 1% of the maximum temperatures registered. The temperature evolution during the thermal cycle is associated with the different process stages as represented in table 3.4.

Table 3.4 Process stages and temperature behaviour.

Process Stage	Plunging	Dwell	Retraction
Temperature Evolution	Heating	Maintenance	Cooling
dT/dt [ºC/s]	$dT/dt > 4$	$-4 < dT/dt < 4$	$dT/dt < -4$

The temperatures reached in FSSW are known to change the base material microstructure in the different weld zones (SZ, TMAZ, HAZ). In the next, based on the temperature evolution with time (thermal cycles), two temperature values were determined in each spot welding test: the maximum temperature (T_{Max}), directly obtained from the raw temperature acquisitions and the maintenance temperature (T_{Man}), obtained by averaging the temperature values in the $-4 < dT/dt < 4$ interval (dwell stage).

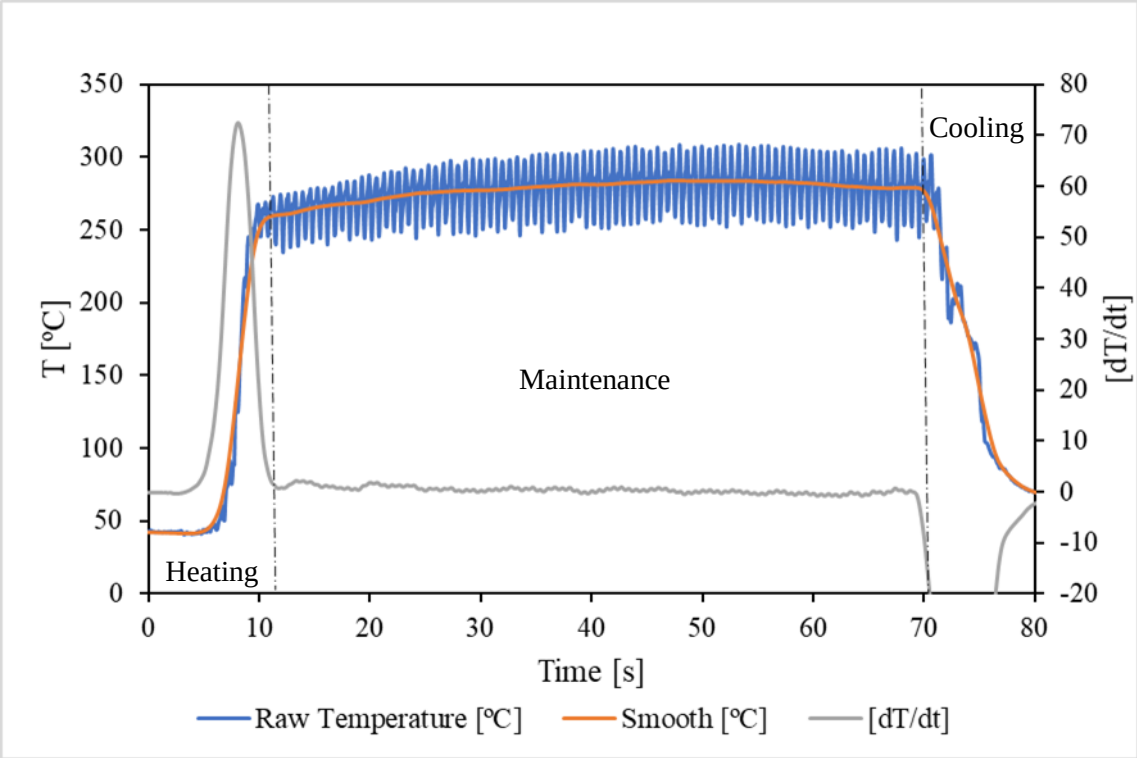

Figure 3.5 Temperature evolution with smooth curve and derivative.

3.5. Torque Acquisition

The torque output signal was captured for every spot welding test with a frequency of 20 Hz. As shown in Figure 3.6 a), due to mechanical vibrations, the raw torque data displayed important noise. A smoothing LOESS functionality from Excel was also used in order to eliminate the noise. The magnification of the torque versus time curve shown in Figure 3.6 b) enables to compare the raw torque data with the smooth curve obtained by post-processing. The figure shows that by reducing the noise, some instantaneous peaks were suppressed from the curves, avoiding the overestimation of the maximum torque associated

to the welding operation. In fact, the post-processing of the torque data enabled to determine two relevant process variables: the maximum torque (M_{Max}), which corresponds to the smooth curve maximum value, and the maintenance or average torque (M_{Man}). In order to be able to correlate the maintenance torque with the maintenance temperature, the same time interval that was considered to calculate these two outputs. That time interval was set using the temperature derivative values between $-4 < dT/dt < 4$, that reflects a stabilization period, as explained in the previous section.

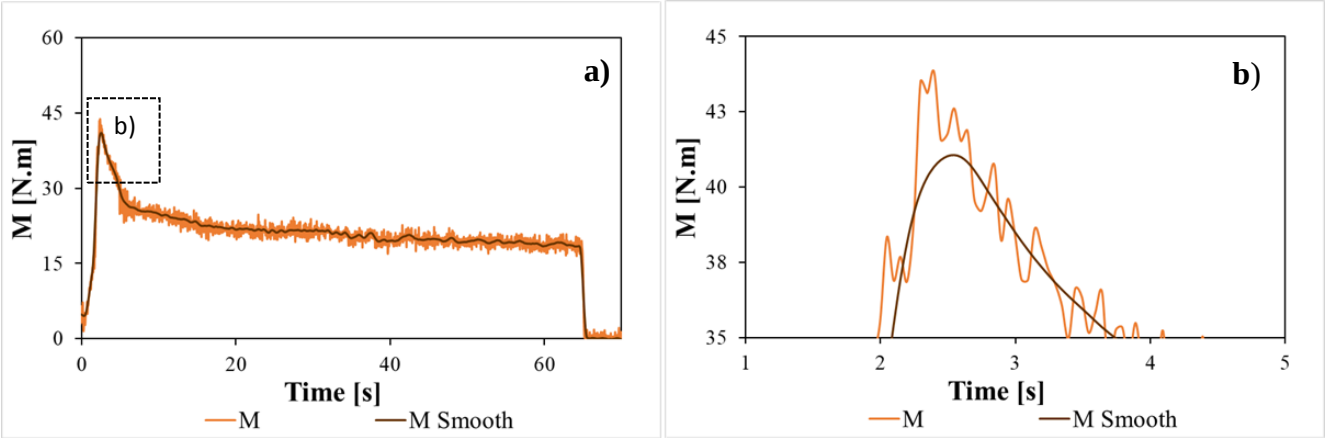

Figure 3.6 a) Torque data and smooth curve application and b) effect of smooth curve on the torque peak.

4. RESULTS AND ANALYSIS

The present chapter begins with a general analysis of the outputs' evolution during the welding operations performed. In the following sections, is then presented a more individualized analysis of the influence of the process parameters and the base materials' properties, on the torque and temperature output data. In the end, is performed a more detailed analysis of the thermomechanical phenomena responsible for the evolution of torque and the temperature with the process parameters.

The temperature and torque versus time curves were plotted, in a single graph, for each spot weld performed, and the maintenance and maximum values of the two outputs were calculated. The results obtained are synthesized in Appendix A.

As shown in the examples of Figure 4.1, some of the tests performed resulted in erratic acquisition profiles of torque and/or temperature, mostly due to errors detected during the experiments, mainly caused by operational issues. In figure 4.1 a) it is possible to see that the torque output reached 0 N.m, during the welding operation. In Figure 4.1 b) it is possible to see that both the torque and the temperature presented an accentuated decrease during the dwell stage. The results of these tests, which presented invalid torque or temperature evolutions with time and, for this reason, were removed from the following analysis, are also listed in Appendix A.

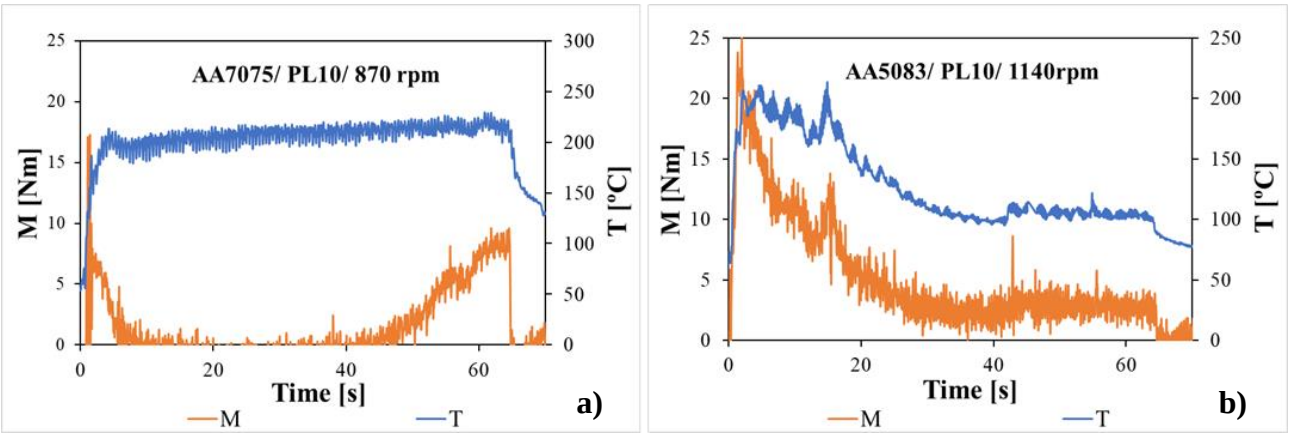

Figure 4.1 Examples of experimental tests containing invalid acquisition data: a) AA7075/ PL18/ 870 rpm and b) AA5083/ PL10/ 1140 rpm

4.1. Outputs Evolution Analysis

In Figure 4.2 are compared the torque and temperature evolutions, with time, for the different base materials. In order to show the similarities in torque and temperature evolutions, observed for the different welding conditions, the results plotted in each graph, in addition of corresponding to different base materials, are also relative to different tools and rotational speeds. In this way, Figure 4.2 a) shows the AA2017 results, obtained using the PL18 tool and 1140 rpm rotational speed, Figure 4.2 b) shows the AA5083 results, obtained using the PL10 tool and 1500 rpm rotational speed, Figure 4.2 c) shows the AA6082 results, obtained using the PL16 tool and 870 rpm, and, finally, Figure 4.2 d) contains the AA7075 results, obtained using the PL12 tool and 660 rpm rotational speed.

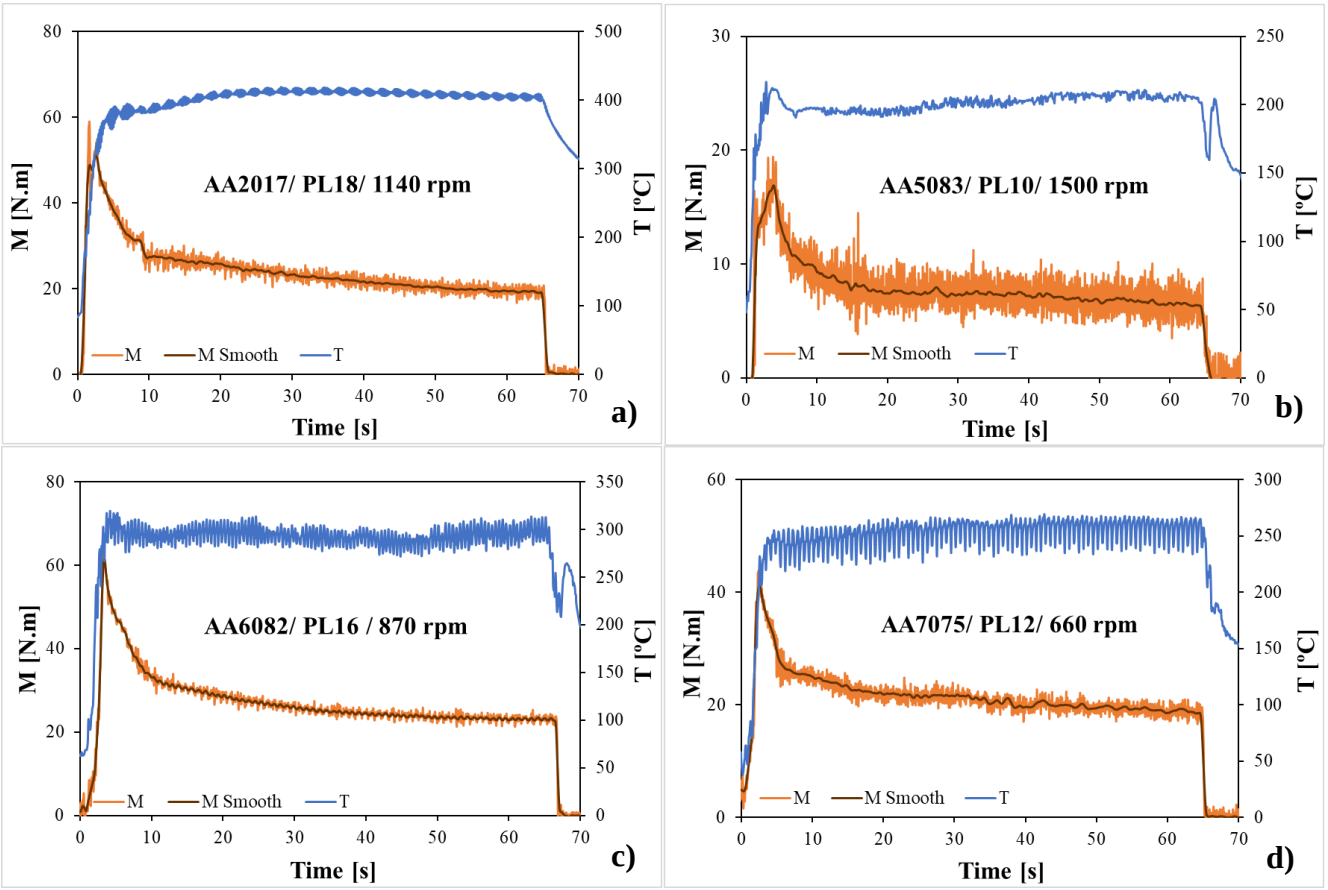

Figure 4.2 Temperature and torque evolution over time for a) AA2017/ PL18/ 1140 rpm, b) AA5083/ PL10/ 1500 rpm, c) AA6082/ PL16/ 870 rpm and d) AA7075/ PL12/ 660 rpm.

Comparing the results plotted in each graph of Figure 4.2, it is possible to conclude that the different curves present similar evolutions over time, despite the changes in the process parameters and base materials. An accentuated increase of torque and temperature occurred in the first 4 seconds of the process, which results from the rapid transitions of the thermomechanical conditions associated with the plunging stage. The initial contact promotes frictional heat generation, which subsequently facilitates plastic deformation, establishing another heat generation source.

After the plunging phase, the tool reaches the predefined plunge depth and, at the same time, the torque reaches its peak value (M_{Max}) as the process enters the dwell stage. During this stage, the temperature values start stabilizing and, at the same time, the torque starts by initially decreasing, until it reaches a maintenance value (M_{Man}) alongside the temperature. At this stage, self-stabilizing thermo mechanical conditions are achieved. After the dwell stage is completed, the tool retracts and the torque and temperature decrease as the process finishes.

Finally, regarding figure 4.2, it is also possible to conclude that, the peak temperatures (T_{Max}) did not diverge significantly from the maintenance temperatures (T_{Man}) values. In fact, the maximum temperatures registered were, on average, 10 to 35 ºC higher than the maintenance temperatures and they were obtained inside the $-4 < dT/dt < 4$ interval. The time required to complete the plunging phase seemed to be enough to fully develop and establish the different heat sources, and when the process entered the dwell stage, the welding conditions converge to a state of thermal balance, giving no large room to temperature variations.

4.2. Temperature Data Analysis

In Figure 4.3 a) to d) is represented the evolution of the maintenance temperature values, with the rotational speed and the shoulder diameter, for the AA2017, AA5083, AA6082 and AA7075 aluminium alloys, respectively.

Analysing the figure, the first conclusion that can be obtained is that, for each base material, there is an important increase in the maintenance temperature with the increase of the shoulder diameter. This happens, since the overall contact area increases with the shoulder dimensions, promoting more frictional and plastic deformation heating. The relationship between the shoulder diameter and the maintenance temperature seems mostly linear when considering shoulder dimensions from 10 to 16 mm, yet an increased influence of the shoulder diameter is observed when its dimensions vary from 16 to 18 mm. For instance, when focusing on the AA2017 alloy (Figure 4.3 a), the increase in maintenance temperature is of about 65 ºC if the shoulder diameter increases from 10 to 12 mm, while an increase of approximately 110 ºC was registered if the shoulder diameter increases from 16 to 18 mm. If considering the AA6082 alloy (Figure 4.3 c), the increase in maintenance temperature is of 50 ºC, if the shoulder diameter increases from 12 to 16 mm, but an increment of about 115 ºC is exhibited if the shoulder diameter is increased from 16 to 18 mm. This effect can also be observed for the remaining alloys, whose results are shown in Figure 4.3 b) and d).

The second conclusion that can be directly extracted from Figure 4.3 is that the influence of changing the rotational speed over the maintenance temperature was almost negligible. As can be seen in Figures 4.3 a), b) and d), relative to the AA2017, AA5083 and AA7075 alloys, respectively, the temperature values for the different rotational speeds are almost overlapped for the different base materials and tool diameters. The only exception to that role was registered for the AA6082 alloy (Figure 4.3 c) while using the PL10 tool. Yet, when considering the higher shoulder diameters, no relevant influence of the tool rotational speed on the temperature can be depicted also for this alloy.

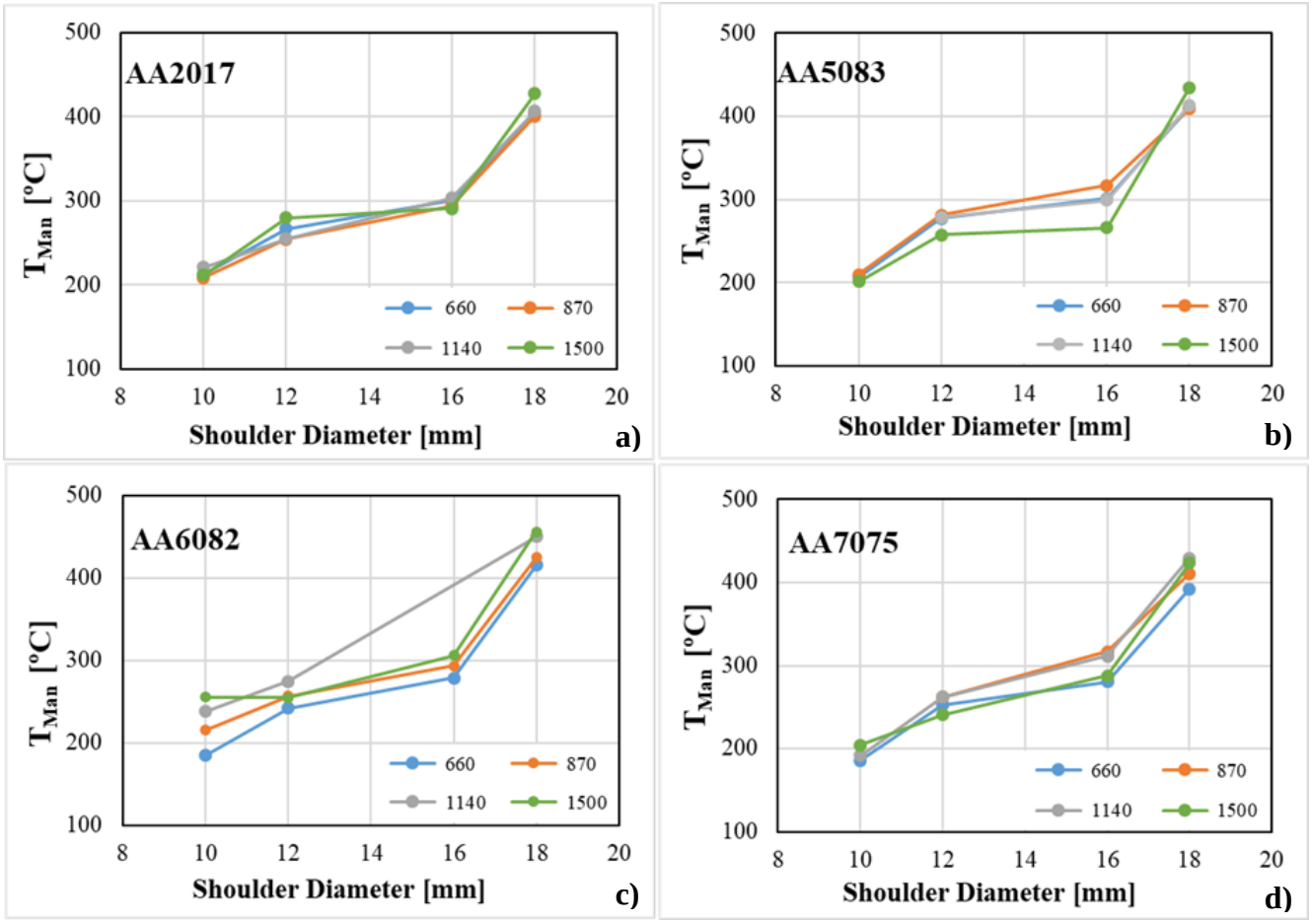

Figure 4.3 T_{Man} Evolution with the process parameters for a) AA2017, b) AA5083, c) AA6082, d) AA7075.

In order to better illustrate the absence of a strong influence of the rotational speed on the maintenance temperatures, in Figure 4.4 two different graphs were plotted containing the thermal cycles registered at different rotational speeds for two fixed base material/tool combinations. More specifically, Figure 4.4 a) shows the temperature data obtained when spot welding the AA7075 alloy, while using the PL12 tool, and Figure 4.4 b) displays the same type of data, but for the AA5083 alloy, while operating with the PL18 tool. Comparing the curves plotted in each figure, it can be concluded that the thermal records are almost overlapped, for both base materials and tools used, despite the change in the rotational speed.

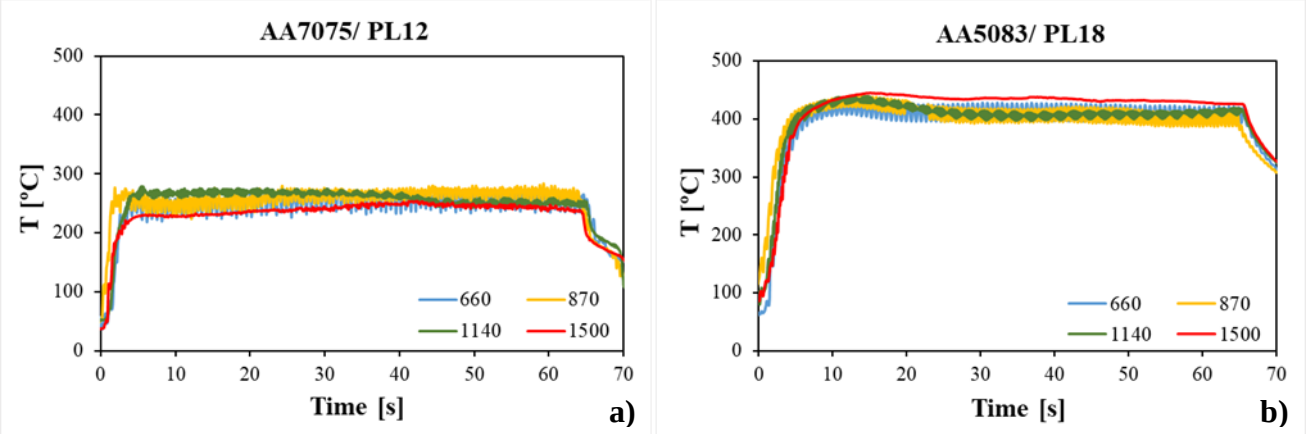

Figure 4.4 Raw temperature output at different rotational speeds for a) AA7075/PL12 and b) AA5083/PL18.

The influence of the base materials' properties on the heat generation was also studied. In Figures 4.5 a) to d) are compared the maintenance temperatures registered for the four different base materials, when welding at rotational speeds of 660, 870, 1140 and 1500 rpm respectively. Comparing the graphics it is possible to conclude that, despite the important differences in strength between the base materials, no important differences in welding temperatures were registered by varying the rotational speeds or shoulder diameters.

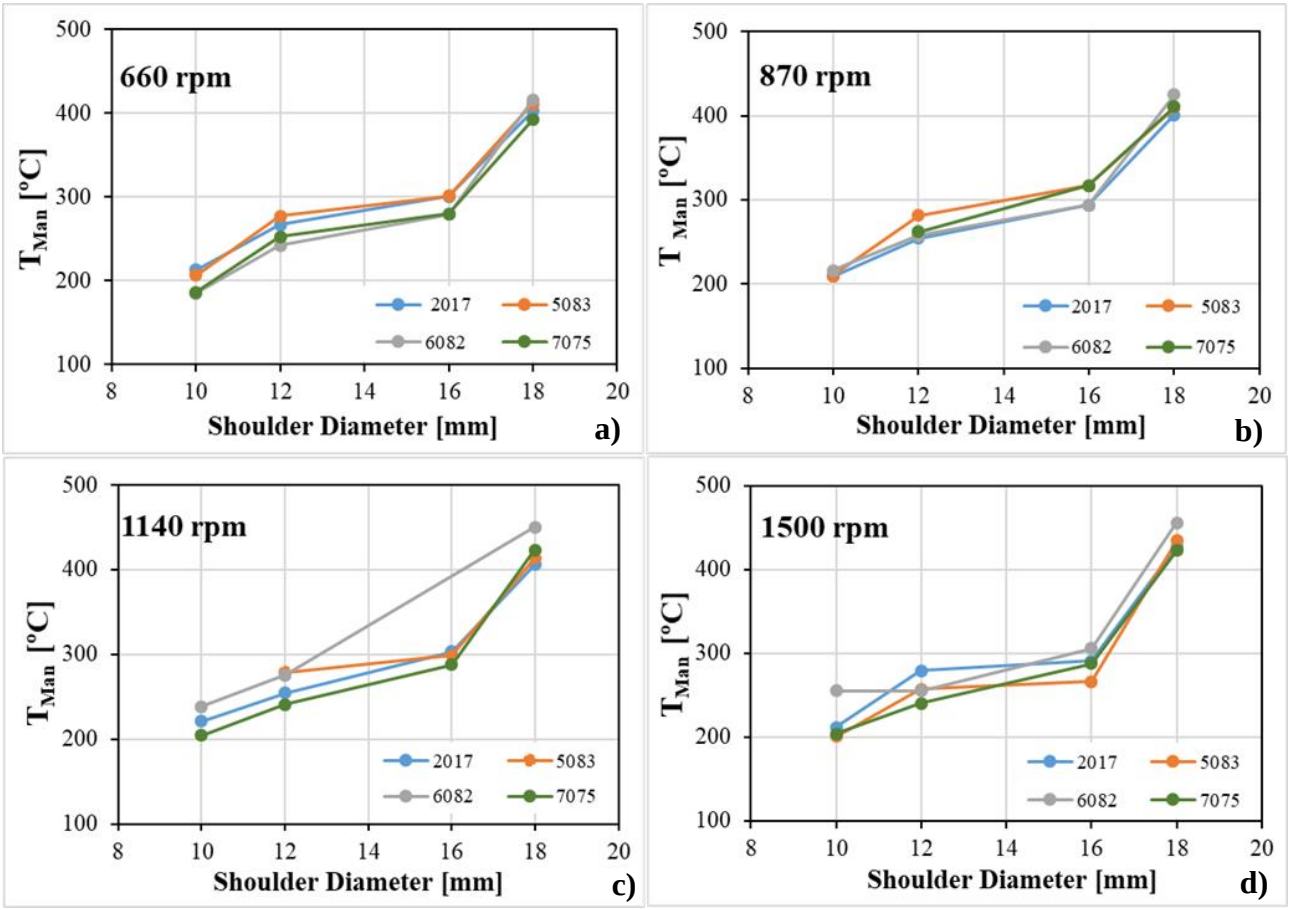

Figure 4.5 T_{Man} evolution for different base materials at a) 660 rpm, b) 870 rpm, c) 1140 rpm and d) 1500 rpm.

4.3. Torque Data Analysis

In figure 4.6 a) to h) is plotted, for each base material, the maintenance (M_{Man}) and the maximum (M_{Max}) torque evolutions, with the rotational speed and the tool dimensions. More precisely, in Figures 4.6 a), c), e) and g) are represented the maintenance torques for the AA2017, AA5083, AA6082 and the AA7075, respectively, while in Figures 4.6 b), d), f) and h) are represented the maximum torques for the alloys previously considered.

Comparing, for each base material, the maximum and maintenance torque values, it is possible to conclude that the maximum torque is always much higher than the maintenance torque. In spite of this, the evolution of both process outputs with the process parameters is very similar. Actually, it is even possible to conclude that the maximum and maintenance torque evolutions, with the process parameters, are similar for the four base materials, i.e., the torque value always decreases for increasing rotational speeds and decreasing tool diameter values. For instance, considering the maintenance torque of AA2017 (Figure4.6 a), if selecting a specific tool, for example PL12, when increasing the rotational speed from 660 to 1500 rpm, the torque decreases from 24.17 to 11.21 N.m. On the other hand, analysing a fixed rotational speed of 660 rpm, torque values increase from 17.97 to 21.32 N.m if the tool is changed from the PL10 to the PL12 and from 30.97 to 35 N.m if the tool is changed from the PL16 to PL18.

The increment in rotational speed is reported to be responsible for inducing higher amounts of heat input, softening the material, which turns the frictional/shearing process more effortless, thus reducing the torque output. Additionally, the increment in the contact area, resulting from the increase in the shoulder diameter, is responsible for generating more frictional stress and larger deformed volumes bellow the shoulder, which will result in an increase in torque output.

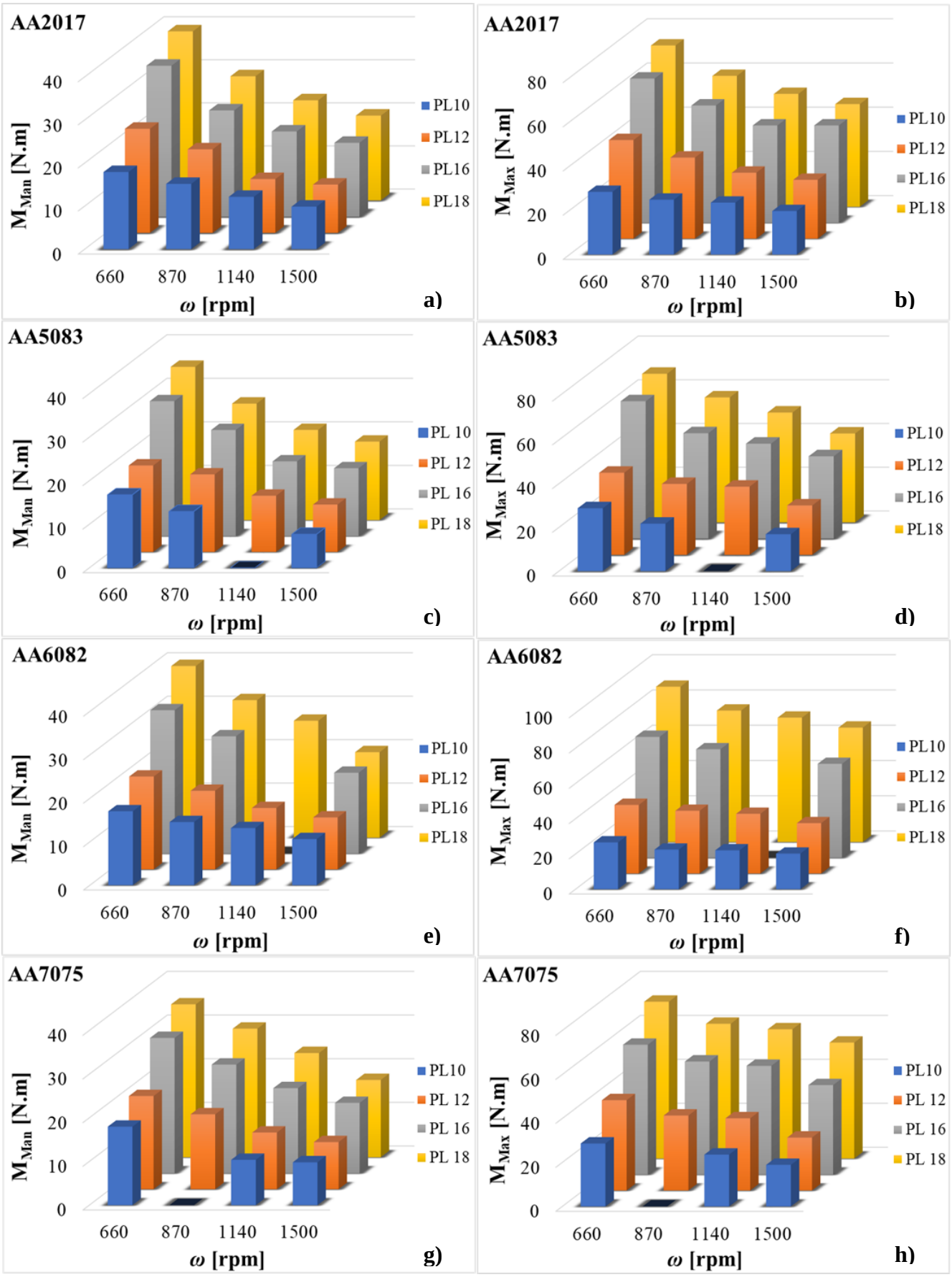

Figure 4.6 Evolution of M_{Man} and M_{Max} with the tool dimensions and rotational speeds for the AA2017 (a and b), AA5083 (c and d), AA6082 (e and f) and AA7075 (g and h).

The influence of the base materials on the maintenance and maximum torque values is better illustrated in Figure 4.7 a) and b) respectively. It can be concluded that no noticeable differences in torque were registered when welding the different base materials. The figures also show that the torque evolution with the tool diameter displays a linear trend, contrary that reported for the temperature evolution. This behaviour is independent of the base material.

Finally, the relative decrease in torque, when increasing the rotational speed from 660 rpm to 1500 rpm, is much higher for the maintenance than for maximum torque. While the maximum torque is a peak value that surges in a shorter amount of time, and its determination is considerably affected by the noise, on the other hand, the maintenance torque, during the dwell stage, has more time to experience the effects of the rotational speed and develop its evolution in accordance.

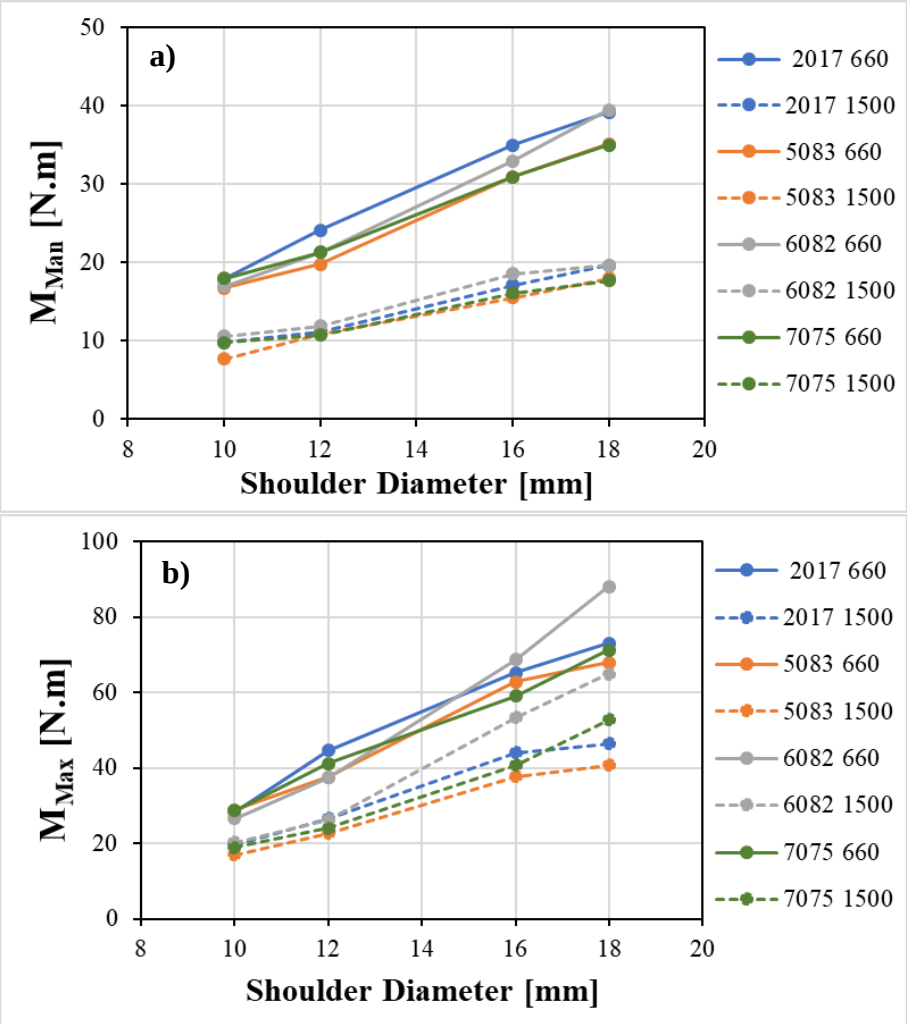

Figure 4.7 Influence of the base material on a) M_{Man} and b) M_{Max} for 660 and 1500 rpm.

4.4. Torque vs Temperature Analysis

In figures 4.8 a) to d) is represented the relationship between the maintenance temperature and the maintenance torque, for the different aluminium alloys. In the graphs are plotted all the results obtained in this work, grouped according to the tool diameter (different colours). Additionally, in each graph, are also plotted two dashed lines, representing the welds produced using the maximum and minimum rotational speeds. Observing the figures, it is possible to conclude that, as the tool dimensions increase, from PL10 to PL18, the influence of the rotational speed on the torque output is higher. For instance, in Figure 4.8 a), for the PL10 tool, the torque gap between the two highlighted rotational speeds has a value of approximately 8 N.m. However, for the PL12, PL16 and PL18 tools, that gap has values of about 14 N.m, 18 N.m and 20 N.m. Similar results can be extracted when analysing the remaining aluminium alloys.

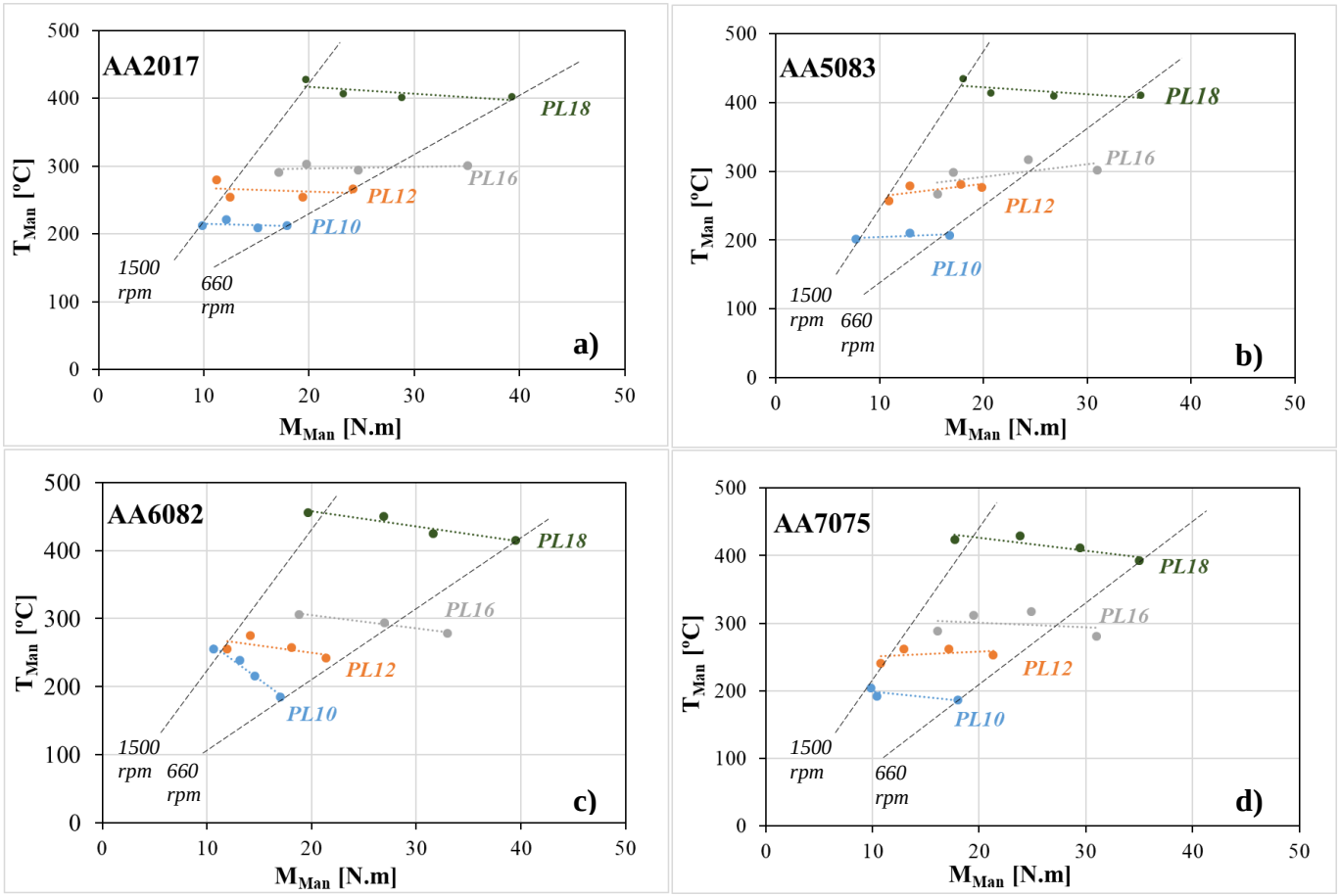

Figure 4.8 T_{Man} vs M_{Man} for a) AA2017, b) AA5083, c) AA6082 and d) AA7075.

Figure 4.8 also shows that, although there is an important decrease in the torque with the rotational speed, in the vast majority of cases, no important temperature differences occurred when changing this process parameter. For instance, for the AA6082 alloy (Figure 4.8 c), considering the PL18 tool, the temperature variation due to the increase of the rotational speed from 660 to 1500 rpm is approximately 40 ºC which represents a 9.8 % variation. Similarly, for the AA7075 alloy (Figure 4.8 d), using the PL10 tool, the temperature increased from 186 to 204 ºC, when varying the rotational speed from 660 to 1500 rpm, which represents an increase in temperature of 9.7%.

In order to better understand the influence of the rotational speed on the thermomechanical conditions that govern the FSSW process, numerical simulations were conducted through the COMET software [45] on the AA6082 aluminium alloy with the PL18 tool using two different rotational speeds, 600 and 1500 rpm. The results of the numerical work are shown in figure 4.9, where it possible to observe the temperature profiles (Figure 4.9 a), the equivalent J_2 stresses (Figure 4.9 b) and the strain rate distributions (Figure 4.9 c) in the cross-sections of pinless spot welds. Analysing the figure it can be concluded that the increase in rotational speed promoted more heat generation. In fact, the temperature variation obtained was of 62 ºC which represented an increase of 12%, similarly to the experimental results. This increase in temperature turned the material much softer, and easy to deform plastically, as can be concluded by analysing the J_2 stresses (Figure4.9 b) and the strain rate distributions (Figure 4.9 c). It seems that, due to the softer properties of the aluminium alloys, the increase in rotational speed, even if producing small changes in temperature, may have a major influence on the plastic deformation mechanisms and consequently, on the torque output.

Analysing the strain rates distribution, it is shown that the increase in rotational speed from 660 to 1500 rpm resulted in an increase of this parameter in 44.5%. It's reported that higher rotational speeds tend to generate more viscous/sticking contact conditions, which are associated to promote heat generation trough plastic deformation at high strain rates [46].

The variation of the J_2 stress values also support the registered decrease in the torque output values due to the increase in the rotational speed. As a matter of fact, while the experimental results registered a maintenance torque decrease of 50.2 % from 660 to

1500 rpm, the numerically obtained J_2 stresses have also decreased approximately 53% between the same rotational speeds.

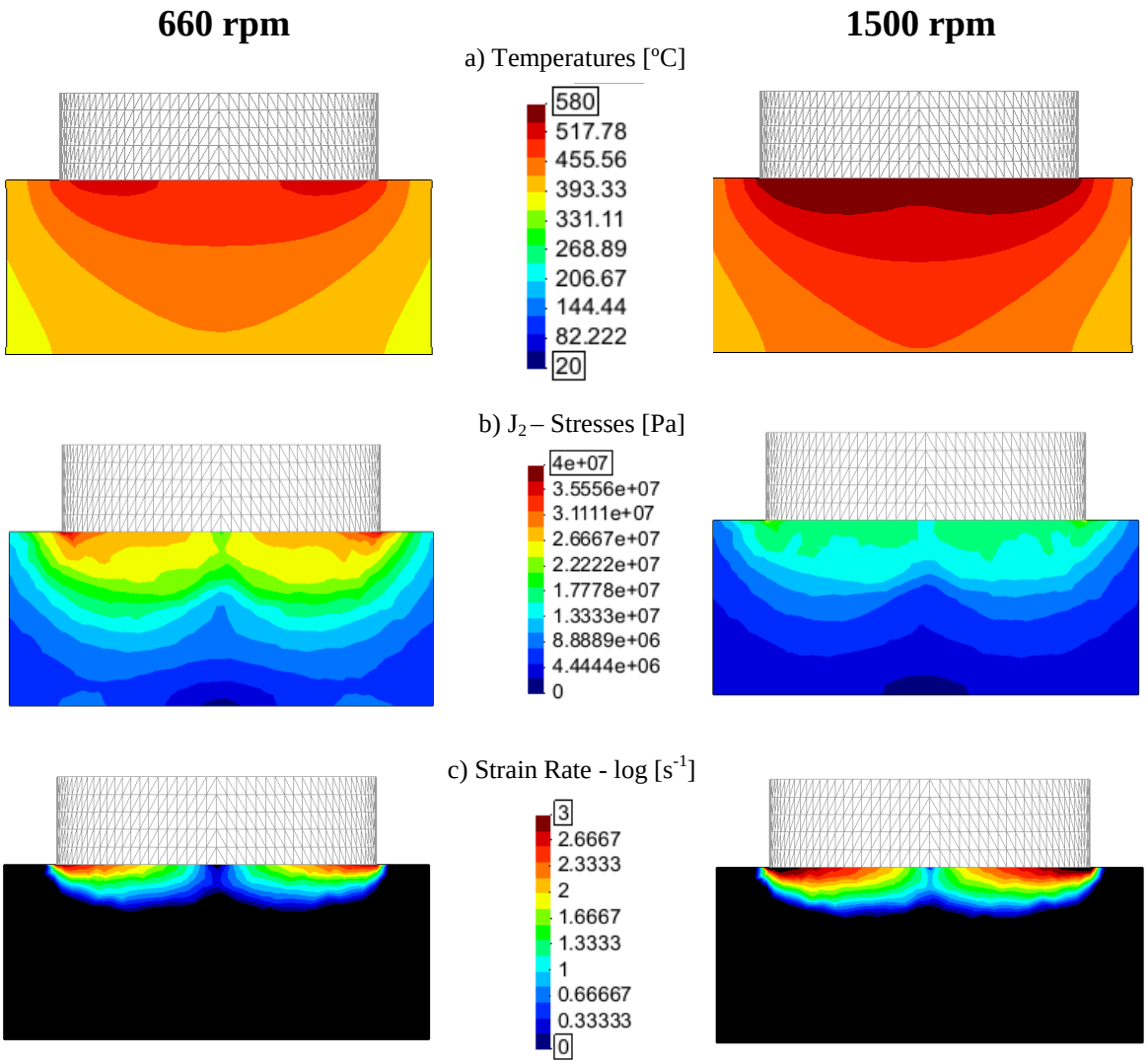

Figure 4.9 Numerical simulation results on the AA6082 using the PL18, for 660 and 1500 rpm: temperature (a), J2-Stresses (b) and strain rate (c) distributions.

The analysis of the evolution of the torque and the temperature was conducted through different approaches. On the following chapter will be presented the modelling, in order to transpose the experimental results into an analytical point of view.

5. MODELING OF TORQUE AND TEMPERATURE

The primary goal of a model is to be able to predict the response of a system to a given change in input. In the current work, the analytical models proposed by Andrade et al. [8] for predicting the torque and temperature in FSW of aluminium alloys, were adapted to be used in the modelling of the same output variables in FSSW. Once reformulated, the models' parameters were determined by fitting them to the experimental results presented in the previous chapter. Later, after defining the analytical equations that express the evolution of the process outputs, these were further treated in the Origin software as a way to represent the models in a more intelligible and extensive way i.e. through Input/Output 3D surfaces, with strong application capability for process monitoring and control.

5.1. The Analytical Models

According to Andrade et al.[8], in order to account for the influence of the tool dimensions on the torque and temperature in FSW, a geometry parameter (G), which quantifies the contact area between the tool and the base material, should be used. For a conventional tool with pin, the G parameter is given by

$$G_{FSW} = \frac{\pi}{4} {D_p}^2 + \pi D_p p_l + \frac{\pi}{4} (D_s - D_p)^2 \quad (1)$$

In which D_p is the pin diameter p_l is the pin length and D_s is the shoulder diameter.

Alongside with the tool dimensions, the traverse speed (v), the plate thickness (t) and the rotational speed (ω) also should be considered in both torque and temperature predictions. Based on this, Andrade et al. [8] purposed two different coefficients to be used in quantifying torque and temperature values. The torque ($C_{M\,FSW}$) and temperature ($C_{T\,FSW}$) coefficients are given by

$$C_{M\ FSW} = \frac{G}{\omega}\sqrt[4]{vt} \tag{2}$$

and

$$C_{T\ FSW} = \frac{G\omega}{\sqrt{vt}} \tag{3}$$

In the current project, both the tool geometry and the process parameters differ from that in conventional FSW. Considering the flat and featureless shoulder geometry, in Eq. (1), only the shoulder diameter (*Ds*) has to be considered, which simplifies the equation as follows

$$G = \frac{\pi}{4}{D_s}^2 \tag{4}$$

In the same way, since in spot welding there is no linear motion of the tool, the traverse speed was also supressed from Eqs (2) and (3). Plate thickness was considered to have influence on heat dissipation and on the torque values obtained by Andrade et al. [8] thus, despite being set as a constant parameter in the present work, it was still introduced on the adapted model with a fixed value of 10 mm, corresponding to the thickness of the plates used to perform the spot welds.

Finally, the analysis conducted in Chapter 4 enabled to conclude that in FSSW, the most influential parameter on the torque evolution and heat generation was the tool diameter. Also, it was concluded that the influence of the tool rotational speed on torque is amplified as the shoulder diameter increases. Based on these assumptions, the torque and the temperature coefficients, in Eqs. (2) and (3), were adapted for the FSSW with pinless tools as follows:

$$C_M = \frac{G}{\omega * \frac{Ds}{10}}\sqrt[4]{t} \tag{5}$$

and,

$$C_T = \frac{G^{\frac{Ds}{10}}\omega}{\sqrt{t}} \tag{6}$$

In these equations, both the torque and the temperature coefficients are now more influenced by the tool dimensions through the term *Ds*/10, which was found, by trial and error, to better adjust the coefficients to the evolution observed experimentally.

5.2. Torque Modelling

In figure 5.1 a) to h) are plotted the experimental torque values versus the torque coefficient, C_M, for all base materials tested. More precisely, in Figures 5.1 a), c), e) and g) are represented the maintenance torque fitting for the AA2017, AA5083, AA6082 and the AA7075, respectively, while in Figures 5.1 b), d), f) and h) are represented the maximum torque fitting for the alloys previously considered. As is shown in the figure, the results were better fitted while using a linear regression. The equations displayed in the graphs may be expressed as follows

$$M = K_M C_M \tag{7}$$

According to Andrade et al. [8], K_M is a constant related to base materials plastic properties. It is also possible to conclude that the C_M was able to provide a satisfactory reproduction of the torque evolution for the chosen experimental conditions. In fact, the Pearson correlation coefficients (R^2) obtained were, on average, 0.94 for M_{Man} and 0.77 for M_{Max}. The fact that M_{Man} reflects a stationary state, while M_{Max} reflects a more rapid transitional state, largely affected by the noise obtained during the welding procedure, may be responsible for the differences in the fitting quality.

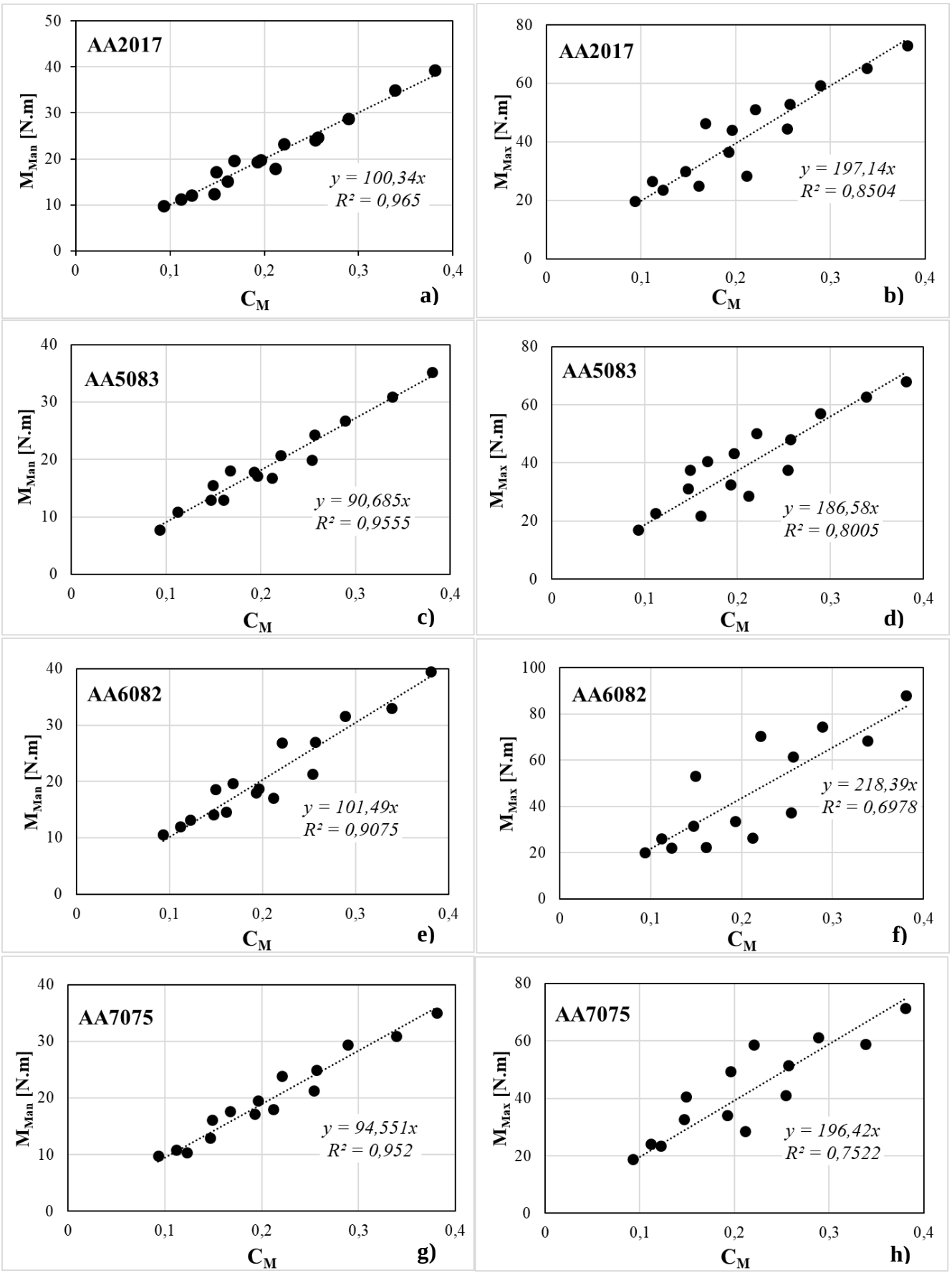

Figure 5.1 C_M Fitting on M_{Man} values for a) AA2017, c) AA5083, e) AA6082, g) AA7075 and on M_{Max} for b) AA2017, d) AA5083, f) AA6082, h) AA7075.

5.3. Temperature Modelling

Since the maintenance and the maximum temperature data proved to be similar, only the maintenance temperature evolution was modelled.

In figure 5.2 a) to d) are plotted the maintenance temperatures, obtained experimentally, against the temperature coefficient C_T. The figures show that the temperature results may be satisfactorily correlated with the C_T coefficient using a power equation:

$$T = K_T C_T{}^{\varphi} \tag{8}$$

According to Andrade et al. [8], in the previous equation, K_T and φ are expected to be related to the material properties responsible for heat generation and dissipation. As shown in the figure, the average Pearson correlation coefficients (R^2) are in the range of 0.87 to 0.93, which indicates that the C_T coefficient was able to successfully reproduce the temperature evolution for the chosen process conditions.

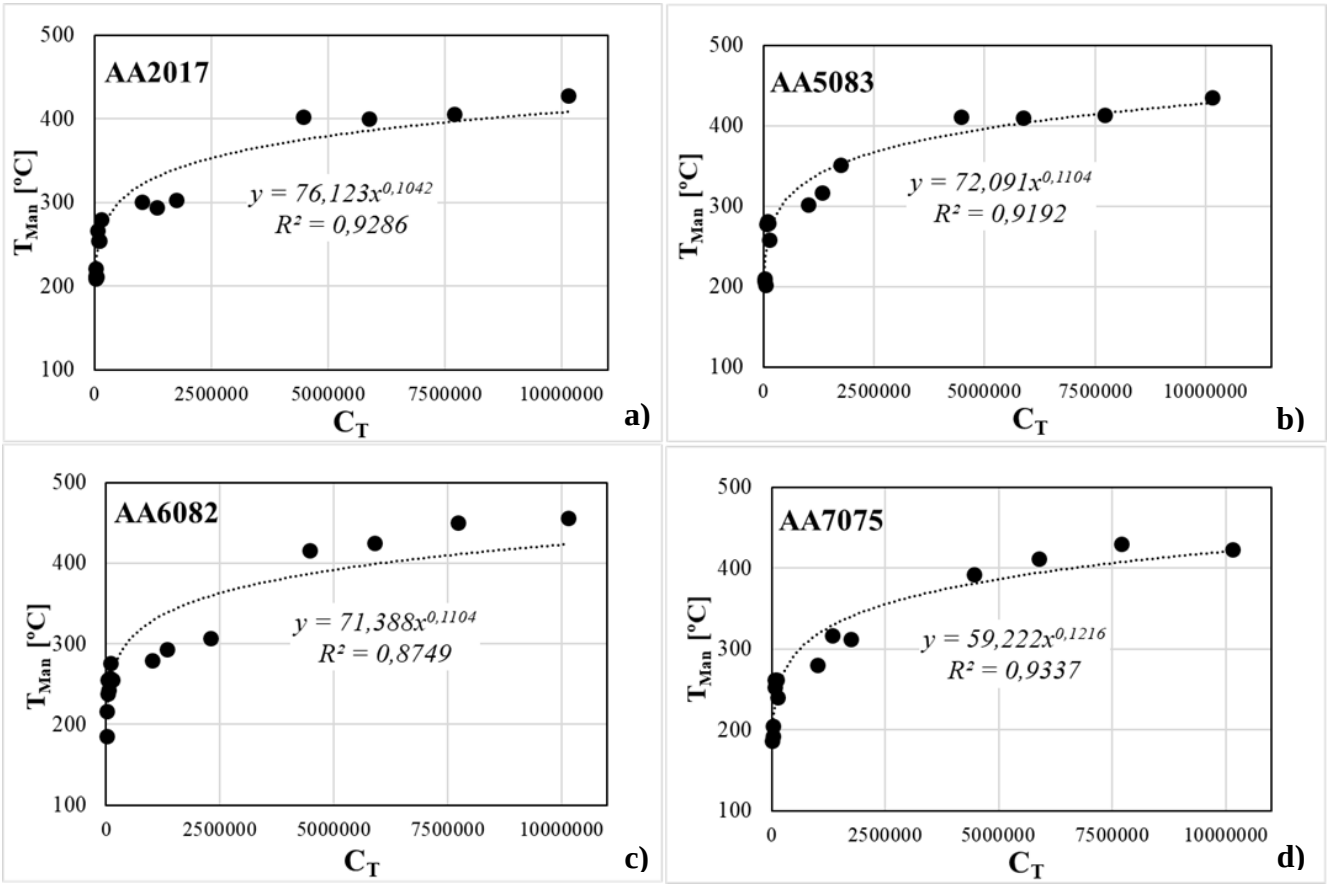

Figure 5.2 C_T Fitting on T_{Man} values for a) AA2017, b) AA5083, c) AA6082 and d) AA7075.

5.4. Input/Output Surfaces

In Figure 5.3 to Figure 5.5 are plotted the generated Input/Output surfaces of the maintenance torque, the maximum torque and the temperature respectively, for each base material. These surfaces were obtained applying the equations in Figure 5.1 and Figure 5.2 to a broader range of shoulder diameters (8 to 20 mm) and rotational speeds (600 to 1600 rpm) than that contemplated in the experimental work. In each plot are also displayed the experimental results as black dots, noticing that, for most of the plots, the faded points are just below the generated surfaces. It´s possible to conclude that the input/output surfaces can satisfactorily reproduce the process outputs for a predetermined shoulder diameter (*Ds*), rotational speed (ω) or base material.

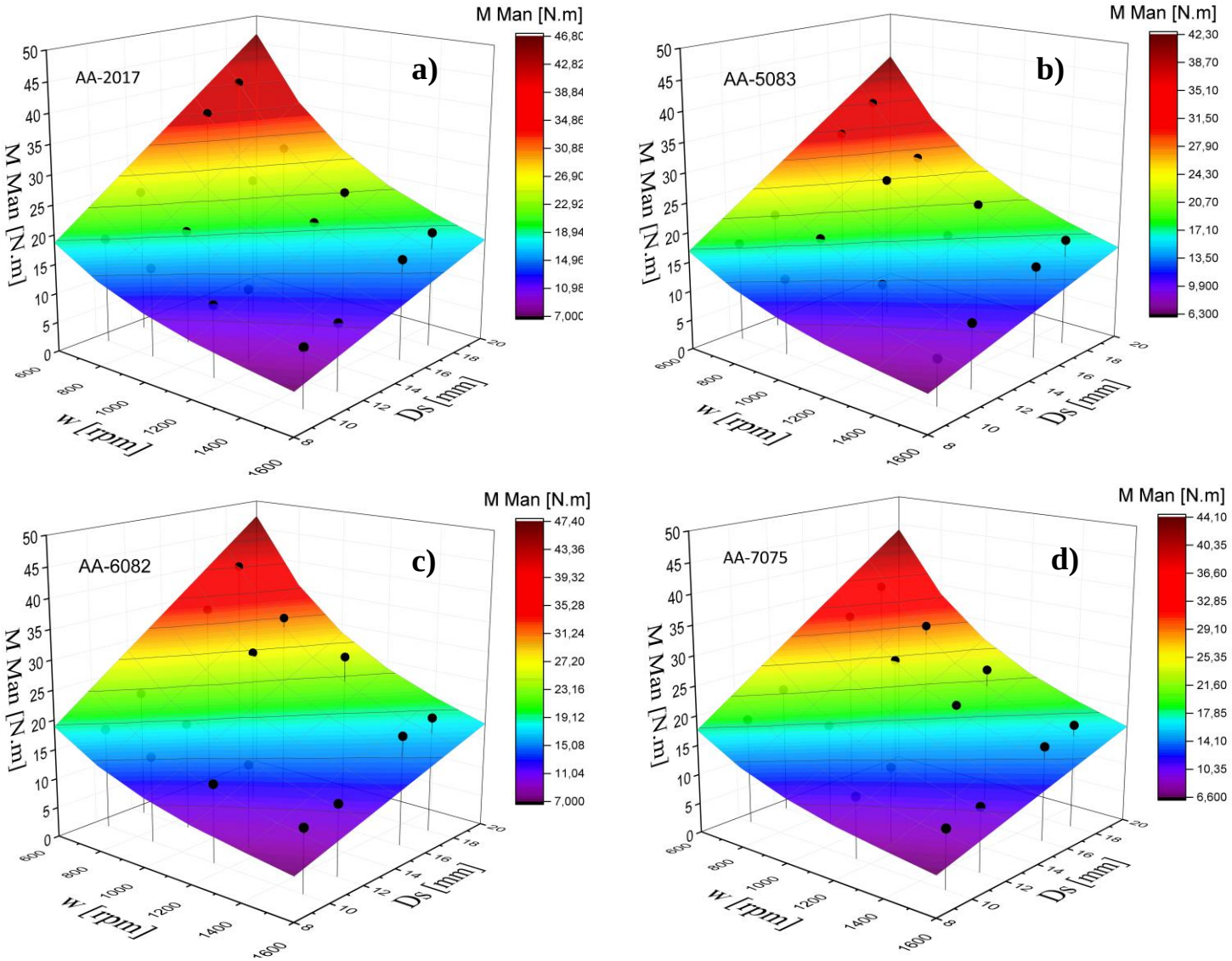

Figure 5.3 Maintenance torque I/O surfaces.

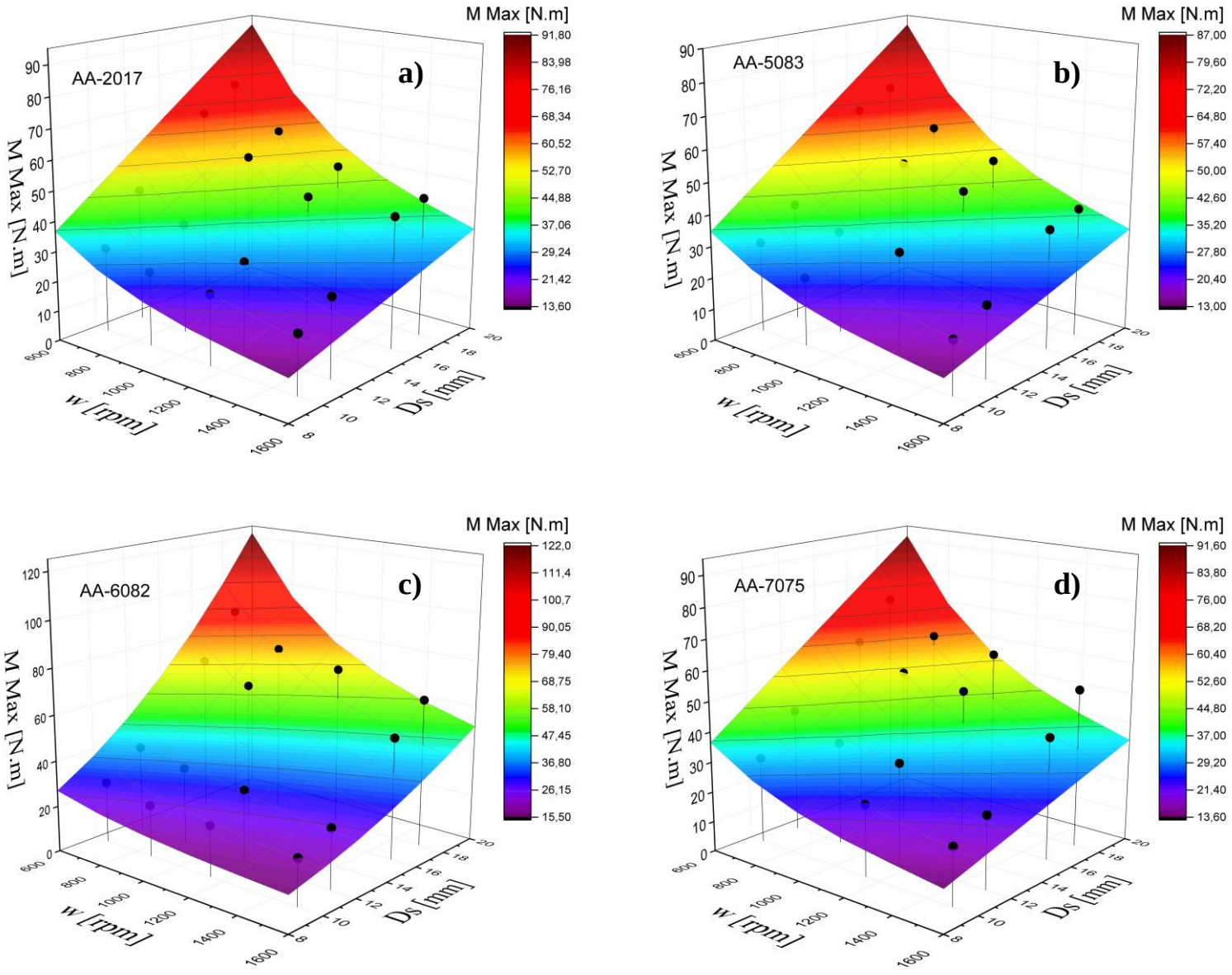

Figure 5.4 Maximum torque I/O surfaces

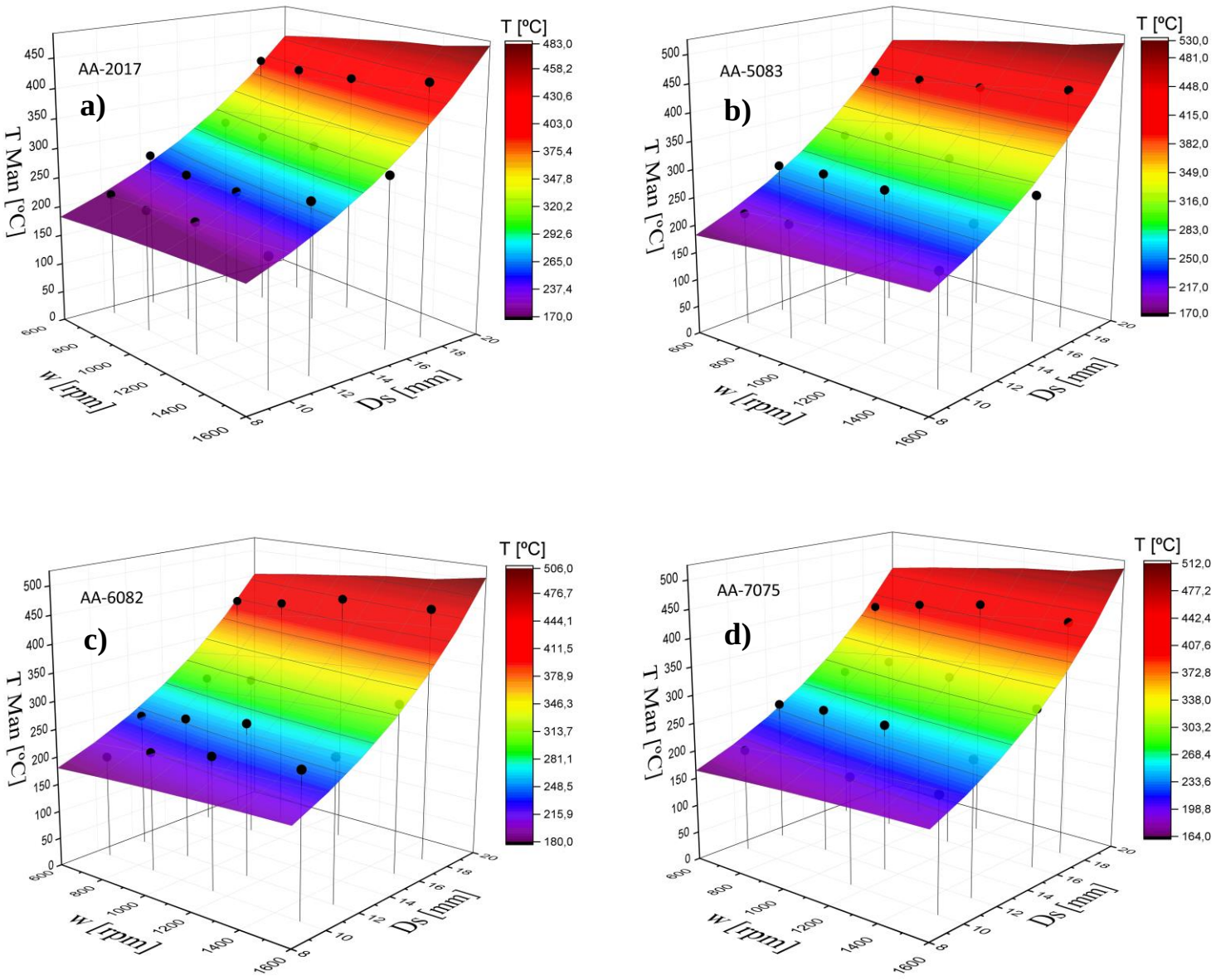

Figure 5.5 Maintenance temperature I/O surfaces.

It is important to emphasize the high level of interest of such representation in which concerns to the monitoring and further control of a productive process, i.e, working as process control maps. In this way, in next sub-chapter, some of the possible applications of those I/O control maps to the pinless FSSW process are discussed.

5.4.1. Application of I/O Control Maps

The generated I/O 3D control maps, can allow the real-time management of the process parameters according to specific welding quality/productive requirements. An example of a practical application of these control maps, can be, for instance, the production of a spot weld in which, the temperature reached, must be between a certain interval, 225 and 325 ºC. If the aluminium alloy intended to weld is the AA2017, then, by limiting the 3D temperature control map, as shown in Figure 5.6, the right combination of process parameters can be optimized in order to reach the required temperatures. In table 5.1 are presented some of the possible process parameters combinations and the corresponding M_{Max} value (obtained from the I/O maximum torque surface). In this way, it will be possible to select the set of parameters according the available welding equipment.

Table 5.1 Possible process parameters combinations that fulfil the temperature boundaries.

Ds [mm]	*ω [rpm]*	M_{Max} *[N.m]*	*T [ºC]*
10	1600	19.06	229.5
12	870	42.1	246.87
12	1500	24.4	261.29
14	600	64.7	274.15
14	1600	26.7	303.6
16	660	73.94	321.5

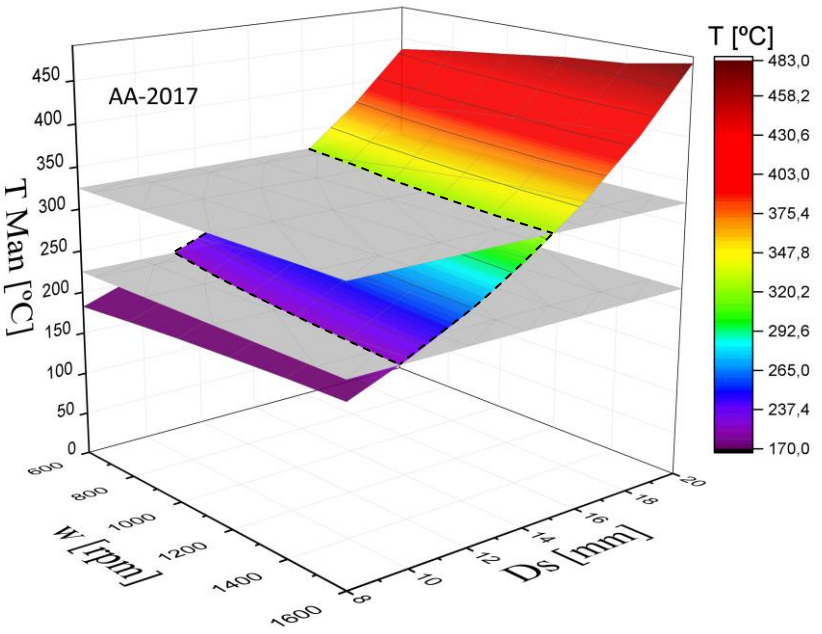

Figure 5.6 Practical application of the I/O Surfaces where the welding temperature is delimited.

Another type of a practical application of this control maps, is if a certain spot welding project is limited by the welding machine maximum torque capacity, for instance, 35 N.m. Assuming that the material supposed to weld is the AA6082, then, as seen in Figure 5.7, by imposing in the M_{Max} control map a maximum value of 35 N.m, it would immediately possible to associate the required process parameters combinations, to the I/O 3D surface area below the grey plane.

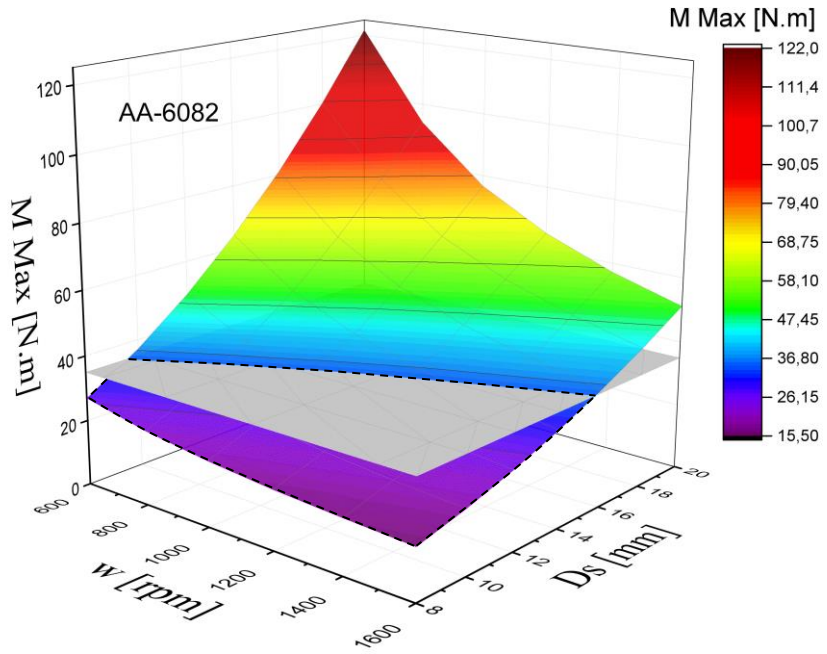

Figure 5.7 Practical application of the I/O surfaces where the welding project is limited by the welding machine maximum torque capacity.

Additionally, the process control maps can also be used to know which is the rotational speed to apply in order to reach a specific temperature value while using a predefined tool. In figure 5.8 is represented the temperature control map of the AA2017, where, for the practical example explained previously, a temperature of 250 ºC and a shoulder diameter of 12 mm are imposed. Under this scenario, the necessary rotational speed to meet these two requirements would be of 980 rpm.

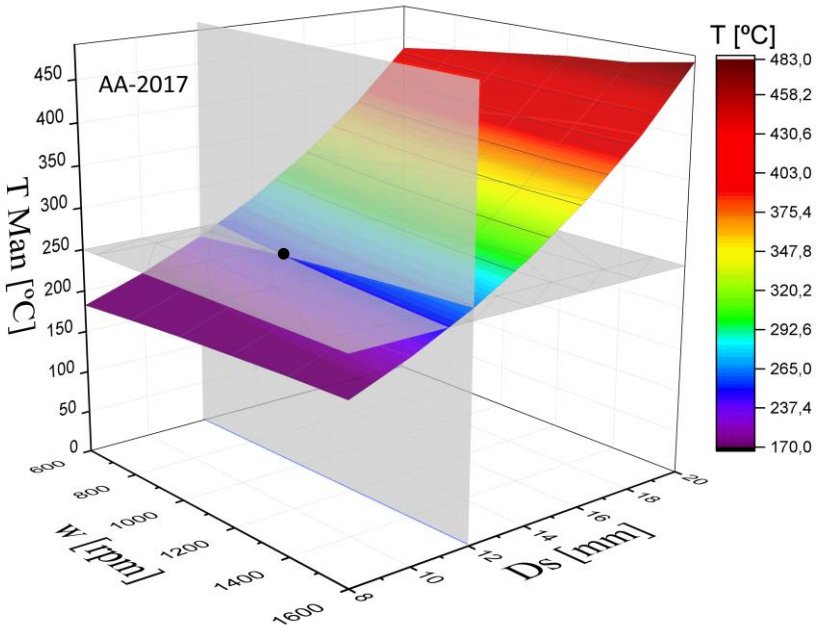

Figure 5.8 Practical application of the I/O surfaces where the project must reach a specific temperature while using a predefined tool.

In each of the suggested practical cases, the maintenance torque control maps could be used as a quality control tool. During the experimental tests, when the machine presented production flaws, those flaws would be directly reflected on the maintenance torque output data. Hence, if the maintenance torque obtained during the production of a spot weld, met the maintenance torque predicted by the M_{Man} control map, it could be assumed that the dwell stage was conducted successfully.

6. CONCLUSIONS AND FUTURE WORK

6.1. Conclusions

The influence of rotational speed, tool dimensions and materials properties on torque and temperature output on the pinless FSSW process was investigated. An adapted analytical model was introduced in order to predict torque and temperature values. The succeeding conclusions were reached:

- Considering the selected set of process parameters, both the torque and the temperature converged to a self-stabilizing condition after the tool reached the imposed plunge depth, independently of base material.
- The torque value is highly sensitive to the rotational speed and the tool dimensions. However, the influence of the rotational speed on the torque output is accentuated by the increase of the shoulder diameter.
- The shoulder diameter is the main parameter governing heat generation while rotational speed showed a minor influence on the temperatures achieved during the dwell stage.
- The different mechanical and thermal properties, associated to the different aluminium alloys studied, had no noticeable impact on torque and temperature values.
- A numerical simulation, also conducted in this work, shown that the decrease in torque for increasing temperatures, promoted by the increase of the tool rotational speed, could be directly related to the evolution of J2 stresses and the strain rates within the welded zone.
- Effective predictions of temperature and torque were assessed by using robust analytical models, with average Pearson Correlation coefficients of 0.94 and 0.91 respectively.
- The proposed Input/Output 3D surfaces satisfactorily replicated the analytical relationships in a more intelligible way. These surfaces have also been pointed as useful tool for future process control.

6.2. Future Work

As suggestions of future work, it's recommended:

- Analysing the cross-sections microstructure and relate the hardness measurements with the temperatures obtained.
- Quantify the plasticized volume and relate it with the process parameters.
- Study the influence of other process parameters such as the plunge depth and the plunge rate.
- Numerical Simulation of the remaining alloys for all conditions tested.
- Study of the actual contact conditions developed during the process and how they could be affected by the process parameters.

BIBLIOGRAPHY

[1] "N. E. Thomas, W. M. Needham, J. C. Murch, M. G. Temple-Smith, P. Dawes, and C. J. US Patent, No., 1995."

[2] K. Y. ALI, "FRICTION STIR WELDING BETWEEN SIMILAR AND DISSIMILAR MATERIALS," *WRIGHT STATE Univ.*, vol. 25, no. 1, pp. 9–14, 2017, doi: 10.1016/j.jpainsymman.2017.04.009.

[3] "FSW TWI - https://www.twi-global.com/technical-knowledge/job-knowledge/friction-stir-welding-147." .

[4] V. M. Magalhães, C. Leitão, and D. M. Rodrigues, "Friction stir welding industrialisation and research status," vol. 1718, no. November, 2017, doi: 10.1080/13621718.2017.1403110.

[5] Y. N. Zhang, X. Cao, S. Larose, and P. Wanjara, "Review of tools for friction stir welding and processing," *Can. Metall. Q.*, vol. 51, no. 3, pp. 250–261, 2012, doi: 10.1179/1879139512Y.0000000015.

[6] C. Leitão, R. Louro, and D. M. Rodrigues, "Using torque sensitivity analysis in accessing Friction Stir Welding/Processing conditions," *J. Mater. Process. Technol.*, vol. 212, no. 10, pp. 2051–2057, 2012, doi: 10.1016/j.jmatprotec.2012.05.009.

[7] S. Guillaume, "Thermal and Mechanical analysis of Friction Stir Welding Process," vol. 1. Universidade de Coimbra, 2019.

[8] D. G. Andrade, N. Dialami, M. Chiumenti, and D. M. Rodrigues, "Using torque as a process control parameter in Friction Stir Welding of Aluminium Alloys," pp. 1–26.

[9] D. Mira-Aguiar, Verdera, C. Leitão, and D. M. Rodrigues, "TOOL ASSISTED FRICTION WELDING: A FSW RELATED TECHNIQUE FOR THE LINEAR LAP WELDING OF VERY THIN STEEL PLATES," *J. Mater. Process. Tech.*, 2016, doi: 10.1016/j.jmatprotec.2016.07.006.

[10] Y. Tozaki, Y. Uematsu, and K. Tokaji, "A newly developed tool without probe for friction stir spot welding and its performance," *J. Mater. Process. Technol.*, vol. 210, no. 6–7, pp. 844–851, 2010, doi: 10.1016/j.jmatprotec.2010.01.015.

[11] R. Rai, A. De, H. K. D. H. Bhadeshia, and T. DebRoy, "Review: Friction stir welding tools," *Sci. Technol. Weld. Join.*, vol. 16, no. 4, pp. 325–342, 2011, doi: 10.1179/1362171811Y.0000000023.

[12] Y. Z. Kan Li, Xuemei Liu, "Research Status and Prospect of Friction Stir Processing Technology," 2019, doi: 10.3390/coatings9020129.

[13] Y. F. Sun and H. Fujii, "Microstructure and mechanical properties of dissimilar Al alloy / steel joints prepared by a flat spot friction stir welding technique," no.

April 2019, 2013, doi: 10.1016/j.matdes.2012.12.007.

[14] "FSSW in Mazda Motor Corp- https://www.assemblymag.com/articles/93337-friction-stir-spot-welding?" .

[15] M. D. Tier *et al.*, "The influence of refill FSSW parameters on the microstructure and shear strength of 5042 aluminium welds," *J. Mater. Process. Technol.*, vol. 213, no. 6, pp. 997–1005, 2013, doi: 10.1016/j.jmatprotec.2012.12.009.

[16] Z. Shen, Y. Ding, and A. P. Gerlich, "Advances in friction stir spot welding," *Crit. Rev. Solid State Mater. Sci.*, vol. 0, no. 0, pp. 1–78, 2019, doi: 10.1080/10408436.2019.1671799.

[17] M. Fujimoto, M. Inuzuka, S. Koga, and Y. Seta, "Development of friction spot joining," *Weld. World*, vol. 49, no. 3–4, pp. 18–21, 2005, doi: 10.1007/BF03266470.

[18] W. Li, J. Li, Z. Zhang, D. Gao, W. Wang, and C. Dong, "Improving mechanical properties of pinless friction stir spot welded joints by eliminating hook defect," *Mater. Des.*, vol. 62, pp. 247–254, 2014, doi: 10.1016/j.matdes.2014.05.028.

[19] D. Bakavos and P. B. Prangnell, "Effect of reduced or zero pin length and anvil insulation on friction stir spot welding thin gauge 6111 automotive sheet," *Sci. Technol. Weld. Join.*, vol. 14, no. 5, pp. 443–456, 2009, doi: 10.1179/136217109X427494.

[20] M. K. Kulekci, U. Esme, and B. Buldum, "Critical analysis of friction stir-based manufacturing processes," *Int. J. Adv. Manuf. Technol.*, vol. 85, no. 5–8, pp. 1687–1712, 2016, doi: 10.1007/s00170-015-8071-5.

[21] X. W. Yang, T. Fu, and W. Y. Li, "Friction stir spot welding: A review on joint macro- and microstructure, property, and process modelling," *Adv. Mater. Sci. Eng.*, vol. 2014, 2014, doi: 10.1155/2014/697170.

[22] A. Gerlich, M. Yamamoto, and T. H. North, "Local melting and tool slippage during friction stir spot welding of Al-alloys," *J. Mater. Sci.*, vol. 43, no. 1, pp. 2–11, 2008, doi: 10.1007/s10853-007-1791-7.

[23] M. Awang and V. H. Mucino, "Energy generation during friction stir spot welding (FSSW) of Al 6061-T6 plates," *Mater. Manuf. Process.*, vol. 25, no. 1–3, pp. 167–174, 2010, doi: 10.1080/10426910903206758.

[24] A. Simar, J. Lecomte-Beckers, T. Pardoen, and B. De Meester, "Effect of boundary conditions and heat source distribution on temperature distribution in friction stir welding," *Sci. Technol. Weld. Join.*, vol. 11, no. 2, pp. 170–177, 2006, doi: 10.1179/174329306X84409.

[25] J. Hodowany, G. Ravichandran, A. J. Rosakis, and P. Rosakis, "Partition of plastic work into heat and stored energy in metals," *Exp. Mech.*, vol. 40, no. 2, pp. 113–123, 2000, doi: 10.1007/BF02325036.

[26] H. Schmidt, J. Hattel, and J. Wert, "An analytical model for the heat generation in friction stir welding," *Model. Simul. Mater. Sci. Eng.*, vol. 12, no. 1, pp. 143–157, 2004, doi: 10.1088/0965-0393/12/1/013.

[27] C. D. Cox, "Friction Stir Spot Welding: Engineering Analysis and Design," p.

270, 2014.

[28] A. Gerlich, G. Avramovic-Cingara, and T. H. North, “Stir zone microstructure and strain rate during Al 7075-T6 friction stir spot welding,” *Metall. Mater. Trans. A Phys. Metall. Mater. Sci.*, vol. 37, no. 9, pp. 2773–2786, 2006, doi: 10.1007/BF02586110.

[29] P. Su, A. Gerlich, T. H. North, and G. J. Bendzsak, “Energy utilisation and generation during friction stir spot welding,” *Sci. Technol. Weld. Join.*, vol. 11, no. 2, pp. 163–169, 2006, doi: 10.1179/174329306X84373.

[30] P. Su, A. Gerlich, T. H. North, and G. J. Bendzsak, “Energy Generation and Stir Zone Dimensions in Friction Stir Spot Welds,” no. 724, 2018.

[31] A. Gerlich, M. Yamamoto, T. Shibayanagi, and T. H. North, “Selection of welding parameter during friction stir spot welding,” *SAE Int. J. Mater. Manuf.*, vol. 1, no. 1, pp. 1–8, 2009, doi: 10.4271/2008-01-0146.

[32] Miroslav Mijajlović and Dragan Milčić, “Analytical Model for Estimating the Amount of Heat Generated During Friction Stir Welding : Application on Plates Made of Analytical Model for Estimating the Amount of Heat Generated During Friction Stir Welding : Application on Plates Made of Aluminium A,” no. January, 2015, doi: 10.5772/53563.

[33] D. M. Neto and P. Neto, “Numerical modeling of friction stir welding process : a literature review,” 2012, doi: 10.1007/s00170-012-4154-8.

[34] H. Badarinarayan, Y. Shi, X. Li, and K. Okamoto, “Effect of tool geometry on hook formation and static strength of friction stir spot welded aluminum 5754-O sheets,” *Int. J. Mach. Tools Manuf.*, vol. 49, no. 11, pp. 814–823, 2009, doi: 10.1016/j.ijmachtools.2009.06.001.

[35] R. Suryanarayanan and V. G. Sridhar, “Process parameter optimisation in pinless friction stir spot welding of dissimilar aluminium alloys using Multi-start algorithm,” *Proc. Inst. Mech. Eng. Part C J. Mech. Eng. Sci.*, vol. 0, no. 0, pp. 1–15, 2020, doi: 10.1177/0954406220919482.

[36] D. G. Andrade, C. Leitão, and D. M. Rodrigues, “In fl uence of base material characteristics and process parameters on frictional heat generation during Friction Stir Spot Welding of steels,” *J. Manuf. Process.*, vol. 43, no. April, pp. 98–104, 2019, doi: 10.1016/j.jmapro.2019.05.015.

[37] D. Bakavos, Y. Chen, L. Babout, and P. Prangnell, “Material interactions in a novel pinless tool approach to friction stir spot welding thin aluminum sheet,” *Metall. Mater. Trans. A Phys. Metall. Mater. Sci.*, vol. 42, no. 5, pp. 1266–1282, 2011, doi: 10.1007/s11661-010-0514-x.

[38] Y. C. Chiou, C. Te Liu, and R. T. Lee, “A pinless embedded tool used in FSSW and FSW of aluminum alloy,” *J. Mater. Process. Technol.*, vol. 213, no. 11, pp. 1818–1824, 2013, doi: 10.1016/j.jmatprotec.2013.04.018.

[39] C. D. Cox, J. R. Aguilar, M. C. Ballun, A. M. Strauss, and G. E. Cook, “The application of a pinless tool in friction stir spot welding : an experimental and numerical study,” vol. 228, no. 11, pp. 1359–1370, 2014, doi:

10.1177/0954407013517374.

[40] X. Yang *et al.*, “Numerical modelling and experimental investigation of thermal and material flow in probeless friction stir spot welding process of Al 2198-T8,” *Sci. Technol. Weld. Join.*, vol. 23, no. 8, pp. 704–714, 2018, doi: 10.1080/13621718.2018.1469832.

[41] W. R. Longhurst, A. M. Strauss, G. E. Cook, and P. A. Fleming, “Torque control of friction stir welding for manufacturing and automation,” 2010, doi: 10.1007/s00170-010-2678-3.

[42] S. E. E. Profile and S. E. E. Profile, “Parametric study of FSSW of aluminium alloy 5754 using a pinless tool,” no. March, 2015, doi: 10.1007/s40194-014-0208-x.

[43] “Base Materials Chemical Compostion - https://www.polylanema.pt/pt/aluminios-tecnicos/.” .

[44] “Materials Specifications - https://www.aerospacemetals.com/aluminum-distributor.html.” .

[45] N. Dialami, M. Chiumenti, M. Cervera, and C. Agelet De Saracibar, “An apropos kinematic framework for the numerical modeling of friction stir welding,” *Comput. Struct.*, vol. 117, pp. 48–57, 2013, doi: 10.1016/j.compstruc.2012.12.006.

[46] D. G. Andrade, C. Leitão, N. Dialami, M. Chiumenti, and D. M. Rodrigues, “Analysis of contact conditions and its influence on strain rate and temperature in Friction Stir Welding,” *Int. J. Mech. Sci.*, p. 106095, 2020, doi: 10.1016/j.ijmecsci.2020.106095.

APPENDIX A

Non considered tests	
Al 5083 – PL10 @1140 rpm	Decrease in torque reaching 0 N.m
Al 6082 – PL16 @1140 rpm	Considerable decrease in temperature
Al 7075 – PL10 @ 870 rpm	Torque presented constant value of 0 N.m during maintenance period

Alloy	Tool	rpm	T Maintenance [ºC]	M Maintenance [N.m]	T Max [ºC]	M Max [N.m]]
2017	PL10	660	212,7819799	17,90197417	235,0023193	28,3775783
		870	208,790524	15,15027726	241,6579895	24,82634297
		1140	220,9955978	12,15027211	259,9693604	23,5008621
		1500	211,7910044	9,867760357	243,3633423	19,6949841
	PL12	660	266,8022579	24,1745473	283,2089539	44,60138151
		870	254,3049324	19,39420755	286,1322327	36,64703291
		1140	254,7910587	12,49712221	301,9347229	29,83003643
		1500	279,7880644	11,20989975	297,6654053	26,58915079
	PL 16	660	300,6771682	35,03380117	319,3025818	65,19334007
		870	294,0317851	24,65507371	325,9157104	53,02364218
		1140	303,2981827	19,77114619	337,2990112	43,98277135
		1500	291,2263264	17,14454529	306,2493286	43,97807843
	PL 18	660	402,5680918	39,23864558	415,4056396	72,96864548
		870	400,8408207	28,82128878	423,5197144	59,20201149
		1140	406,2823998	23,23266581	419,5392151	51,03961015
		1500	427,6613201	19,67674704	445,6916809	46,43115692
5083	PL10	660	206,6989502	16,7607422	226,5483093	28,77520582
		870	209,8448842	12,9384933	234,879425	21,69237965
		1140				
		1500	201,2529026	7,715125414	216,3985138	16,87466658
	PL12	660	277,2284248	19,84780738	308,9208069	37,54710514
		870	281,4611182	17,80207796	313,0848694	32,45209617
		1140	278,7508701	12,90424931	296,2096252	31,19235406
		1500	257,6072187	10,87680422	264,4484253	22,60150221
	PL 16	660	301,4327624	30,94988335	331,1043396	62,80746939
		870	317,111396	24,34568	334,26828	48,19677513
		1140	299,1475648	17,13281195	351,6462708	43,41150686
		1500	266,5145271	15,55892768	279,0052185	37,6496521
	PL 18	660	411,2842618	35,18780093	430,0378418	67,94309952
		870	409,7386068	26,75239531	439,7624512	57,13274033
		1140	413,8146831	20,70511847	440,543335	50,21591447
		1500	434,6982218	18,02077345	444,8521423	40,61702293

Alloy	Tool	rpm	T Maintenance [ºC]	M Maintenance [N.m]	T Max [ºC]	M Max [N.m]]
6082	PL10	660	185,3701975	17,01977171	219,7510681	26,58635916
		870	216,1268725	14,54096205	249,4194031	22,49641578
		1140	238,4833417	13,14695727	267,3001404	22,09243757
		1500	255,7656478	10,61322298	264,3157349	20,20347936
	PL12	660	242,4999851	21,36320848	269	37,44012031
		870	257,4220773	18,07409073	283,4623718	33,65903553
		1140	275,4635452	14,11818068	309,1768494	31,54090165
		1500	255,3482795	11,94229341	279,9369507	26,29733071
	PL 16	660	279,0458599	32,9715957	293,7960815	68,59692301
		870	293,5726367	26,97595446	319,3526611	61,556824
		1140				
		1500	306,4826422	18,58327249	317,8313599	53,26755691
	PL 18	660	415,4970203	39,49135764	425,777771	88,11101101
		870	424,8280685	31,63777597	435,4950256	74,59172225
		1140	450,3595783	26,88600857	464,4950867	70,57436217
		1500	456,2191925	19,66655955	463,466217	64,91374974
7075	PL10	660	186,2103478	17,97449865	207,4904785	28,64528694
		870				
		1140	191,8178472	10,38250087	220,6267395	23,5923447
		1500	204,4377041	9,816830981	224,908844	18,93335139
	PL12	660	252,8585598	21,32426598	268,934082	41,07596691
		870	262,0534295	17,14101398	283,1002808	34,08738537
		1140	261,9048558	12,9743483	279,5352783	32,8202236
		1500	240,7892495	10,78844912	254,1373291	24,06429555
	PL 16	660	280,3229496	30,97049318	302,0907593	58,9811463
		870	317,0497339	24,87192944	336,0438843	51,37288226
		1140	311,7017702	19,47117038	330,3712463	49,40776455
		1500	287,9234253	16,10598278	293,1419678	40,6480855
	PL 18	660	392,691774	35,00657789	412,813385	71,26984447
		870	411,1005233	29,43925929	422,6467285	61,25362361
		1140	429,7728755	23,86208883	437,5729065	58,75435343
		1500	423,2930087	17,69355768	435,7026844	52,69391963